Predicting the effects of hypoxia on oyster (*Crassostrea virginica*) growth and reproduction through the Dynamic Energy Budget model

Anna Manyak Davis[1*], Katherine McFarland[2], Louis V. Plough[3], Kennedy T. Paynter[1,4,5]

[1] Marine-Estuarine-Environmental Science, University of Maryland College Park, College Park, MD, USA

[2] National Oceanic and Atmospheric Administration Milford Lab, Milford, CT, USA

[3] Horn Point Laboratory, University of Maryland Center for Environmental Science, Cambridge, MD, USA

[4] Department of Biology, University of Maryland College Park, College Park, MD 20742, USA

[5] Chesapeake Biological Laboratory, University of Maryland Center for Environmental Science, Solomons, MD, USA

* Corresponding author. Present address: Smithsonian Environmental Research Center, Edgewater, MD 21037, USA

Email addresses: DavisAM@si.edu (A.M. Davis), Katherine.McFarland@noaa.gov (K. McFarland), LPlough@umces.edu (L.V. Plough), Paynter@umd.edu (K.T. Paynter)

Abstract

Hypoxia in the world's oceans poses an increasing threat to marine organisms and ecosystems, and there is a need to scale individual effects in order to make predictions about the broader ecological consequences of reduced oxygen availability. Mechanistic models, such as the Dynamic Energy Budget (DEB) model, provide a useful framework for quantifying the effects of changing environmental conditions, such as hypoxia, on individual organismal response. While the standard DEB model is forced solely by temperature and food availability, recent additions to the model for some marine species have allowed for the modulation of DEB energy fluxes in response to oxygen availability. The eastern oyster, *Crassostrea virginica*, is a sessile marine invertebrate inhabiting coastal environments experiencing variability in oxygen availability for which a DEB model has already been parameterized, but dissolved oxygen has not yet been incorporated as a forcing variable. The present study uses observed oyster growth data from sites throughout the Chesapeake Bay experiencing a range of oxygen regimes to validate a DEB model for *C. virginica*, implementing a constraint on energy fluxes due to oxygen availability. The effect of dissolved oxygen is parameterized into the *C. virginica* DEB model using an oxygen correction factor to constrain assimilation, mobilization, and ingestion rates within the energy budget. The resulting model accurately predicts empirically measured oyster growth data, with an average deviation between simulated and observed shell lengths of 4.70% across all sites assessed. The model is then used to make predictions about hypoxia's influence on growth and reproduction over the oyster's growing season using data from two additional sites in the Chesapeake Bay. Model outputs indicate that low oxygen exposure results in reduced growth for oysters, in both shell length (6.9% reduction) and tissue mass (23.6% reduction), as well as reductions in oyster fecundity (54.4% reduction in number of eggs spawned) and alterations to

spawning frequency during the summer, which collectively has the potential to negatively affect oyster ecology. Overall, the integration of dissolved oxygen into the *C. virginica* DEB model provides an important tool to make predictions about how oysters will respond to future oceanic and coastal deoxygenation.

Keywords: Dynamic Energy Budget, hypoxia, *Crassostrea virginica*, oyster, modeling, Chesapeake Bay

1. Introduction

Oxygen availability in coastal and open ocean waters is expected to decrease in the coming decades as a result of increased nutrient input to coastal waters and rising water temperatures, which will both reduce oxygen solubility and increase the intensity of water column stratification (Breitburg et al. 2018). Low oxygen availability or hypoxia – broadly defined as dissolved oxygen concentrations less than 2.0 mg/l (Rabalais et al. 2010) – is a significant threat to marine organisms, particularly sessile marine bivalves which lack the motility to escape deoxygenated waters. On an individual level, exposure to hypoxia in bivalves causes decreased ingestion rates (Wang and Widdows 1993, Sobral and Widdows 1997, Clark 2014), decreased respiration rates (Taylor and Brand 1975, Shumway and Koehn 1982, Hicks and McMahon 2002), decreased growth rates (Stevens and Gobler 2018), reduced reproductive potential (Long et al. 2014), and mortality (Stickle et al. 1989, Hicks and McMahon 2005, Gobler et al. 2014). These individual responses to hypoxia can collectively result in broader ecological implications, among them increased incidence of predation (Nestlerode and Diaz 1998), alterations to community diversity (Diaz and Rosenberg 1995), and effects on population structure (Marcus et al. 2004, Eby et al.

2005). Given the growing threat of hypoxia, the ability to translate the individual effects of hypoxia into broader population and life history effects is important in order to make predictions about how reduced oxygen availability will influence organisms and ecosystems over longer timescales.

The use of mechanistic modeling offers a means to quantify and predict individual responses to hypoxia, which otherwise might be logistically prohibitive to measure empirically. One such model, the Dynamic Energy Budget (DEB) model (Kooijman 1986, Kooijman 2000, Kooijman 2010), is a generalized framework for quantifying how energy is utilized in heterotrophic and autotrophic organisms. Because DEB theory was conceived to provide a unifying framework to describe energy utilization in all heterotrophs, it is broadly applicable for use with terrestrial or marine organisms. The DEB model quantifies organismal energy ingestion and allocation towards growth, development, maintenance, and reproduction, leading to predictions about the effects to the energy budget, which includes growth and reproduction. For the standard DEB model, food availability and temperature drive the dynamics of the system. However, in recent years, research in marine organisms specifically has expanded the model's use to understand effects of environmental stressors on organismal life history traits, including toxicants (Galic et al. 2017), low salinity (Lavaud et al. 2017), and low dissolved oxygen (Aguirre-Velarde et al. 2019a, Lavaud et al. 2019).

Given oxygen's importance for energy production in aerobically respiring organisms, hypoxia has the ability to affect many aspects of an organism's energy budget (reviewed by Thomas et al. 2019). Exposure to low oxygen reduces filtration and ingestion rates in filter-feeding bivalves,

reducing the influx of energy into the organism (Sobral and Widdows 1997, Hicks and McMahon 2002, Clark 2014). The assimilation of energy from ingested food into utilized energy can also be reduced under low oxygen exposure due to reductions in the activity of enzymes necessary for energy assimilation (Wang et al. 2011). Of the energy assimilated, hypoxia can hinder the ability of organisms to mobilize energy reserves because facultative anaerobiosis – undertaken by organisms under hypoxia stress – results in reduced energetic outputs (Aguirre-Velarde et al. 2019a). The consequences of these energetic effects are reductions in growth (Baker and Mann 1992, Gobler et al. 2017, Stevens and Gobler 2018) and reproduction (Long et al. 2014, Aguirre-Velarde et al. 2019b).

The eastern oyster, *Crassostrea virginica*, is a wide-ranging coastal bivalve providing critical ecosystem services to the waters it inhabits, such as water filtration (Coen et al. 2007), coupling benthic-pelagic dynamics (Smyth et al. 2013), and structural habitat for other marine organisms (Grabowski and Peterson 2007). Populations of *C. virginica* have suffered significant declines in abundance over the last century due to overharvesting, disease, and reduced water quality (Jackson et al. 2001, Kirby 2004). Throughout its range, *C. virginica* is exposed to low oxygen availability on hourly, daily, and seasonal timescales (e.g., Breitburg 1990, Dame 1979), and although oysters generally show high overall tolerances to hypoxia compared to other marine invertebrates (Stickle et al. 1989), hypoxia still poses a threat to the health of *C. virginica* populations. Hypoxia exposure has been shown to reduce oyster larval settlement (Widdows et al. 1989), increase susceptibility of oysters to disease (Keppel et al. 2015), and lead to mass mortalities of adult oysters (Johnson et al. 2009). As the frequency of hypoxic events continues to increase in the Chesapeake Bay (Ni et al. 2019) and other areas that *C. virginica* inhabits (e.g.

93 Laurent et al. 2018), the development of mechanistic models, such as the DEB model, to predict
94 potential consequences of hypoxic exposure for organismal life history traits is critical.
95
96 Energetic constraints related to dissolved oxygen have previously been integrated into DEB
97 models developed for Atlantic cod, *Gadus morhua* (Lavaud et al. 2019), and Peruvian scallop,
98 *Argopecten purpuratus* (Aguirre-Velarde et al. 2019a), using an oxygen correction factor. In
99 both studies, the oxygen correction factor, driven by a species-specific critical oxygen
100 concentration, was used to modulate energetic fluxes within the energy budget. For Atlantic cod,
101 the oxygen correction factor acted solely on ingestion rates, reducing ingestion along with
102 declining oxygen tension until a critical oxygen concentration, under which ingestion ceased. In
103 contrast, for the Peruvian scallop, the energetic response to oxygen concentrations was based off
104 of their oxygen consumption rates under declining oxygen and was treated as a two-phase
105 response, with energy assimilation and mobilization fluxes decreasing linearly below a critical
106 oxygen concentration. Similar to the Peruvian scallop, *C. virginica* displays a two-phase
107 response in oxygen consumption under declining dissolved oxygen concentrations (Shumway
108 and Koehn 1982). At higher oxygen concentrations, *C. virginica* oxyregulate, maintaining
109 relatively constant levels of oxygen uptake despite the concentration of oxygen in the
110 environment. However, below a critical oxygen concentration, they oxyconform, reducing their
111 oxygen consumption as they begin to undergo anaerobic respiration (Shumway and Koehn
112 1982). Given the similar physiological response to oxygen in *C. virginica*, the method of
113 modulating energy fluxes with an oxygen correction factor used in the study with *A. purpuratus*
114 is likely transferable to the eastern oyster.
115

The goal of the present study was to explicitly integrate dissolved oxygen into the DEB model developed for *C. virginica* (Lavaud et al. 2017) to provide a tool for predicting the broader energetic and life history implications of reduced dissolved oxygen on *C. virginica*. To accomplish this, the effect of dissolved oxygen was first parameterized into the *C. virginica* DEB model using an oxygen correction factor to constrain assimilation, mobilization, and ingestion rates within the energy budget. After model validation, the model was then used to predict oyster growth and reproductive output at two sites in the Chesapeake Bay that differ in summertime oxygen availability to understand the effects of reduced oxygen on oyster life history traits over the course of the oyster's growing season. The development of this model and the understandings of individual organismal effects that could be gleaned from its use has the potential to yield important insights into how oyster populations in the Chesapeake Bay currently respond to hypoxic conditions and predict responses to future oxygen scenarios.

2. Methods

2.1 Dynamic Energy Budget Model

The model used in this study is based on the Dynamic Energy Budget (DEB) theory (Kooijman 2010). The generalized DEB theory describes the flow of energy from ingestion of food from the environment into the organism for use in growth, maintenance, development, and reproduction (Figure 1). The model uses four state variables to describe the flow of energy through an individual: reserves (E), structural volume (V), reproduction (E_R), and gametes (E_{GO}). A portion of ingested energy is assimilated into reserve energy. From there, a fixed fraction of energy (κ) is partitioned towards structural growth and somatic maintenance, while the remaining fraction of

energy $(1-\kappa)$ is partitioned in juveniles towards maturation and in adults towards reproduction and reproductive maintenance costs. Some of the energy allocated for reproduction in adults is stored in and eventually released as gametes.

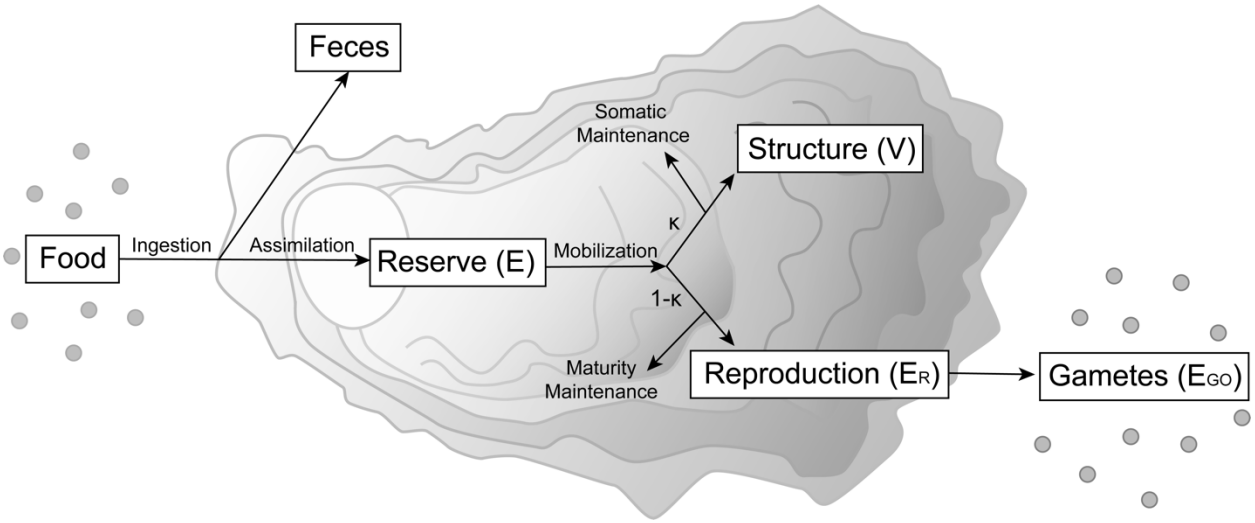

Figure 1: Conceptual diagram of the DEB model. Oyster vector image from Tracy Saxby (UMCES Integration and Application Network media library).

The model used in the present study was built on the standard DEB growth model parameterized for *C. virginica* by Bernard et al. (2011) and Lavaud et al. (2017). Each model run represented growth of a single individual using fixed parameters. Growth time steps occurred every fifteen minutes (in accordance with the environmental data time step) and growth was calculated using DEB model differential equations for the four state variables (reserves, structural volume, reproduction, and gametes). Specific equations used in the model are listed in Table 1. Parameter values were primarily sourced from Lavaud et al. (2017) and Lavaud et al. (2021) (which were further validated by Lavaud et al. [2024]), while others were identified from primary literature (described below). The parameters used in the model as well as the source from which the value was obtained can be found in Table 2. All statistical analyses and model simulations were carried

out in R (Version 3.6.1 / RStudio Version 1.3.1073). Model simulations were run using a publicly available R script (Monaco et al. 2019), customized for use with the *C. virginica* DEB model developed here.

The standard DEB model is forced by environmental food availability and temperature, the former driving ingestion rates and the latter affecting ingestion, mobilization, and maintenance rates. Recently, salinity was incorporated as an additional forcing variable in the *C. virginica* growth model using a salinity correction factor (C_S) acting on ingestion rates ($\dot{p}_X$, Lavaud et al. 2017). The correction factor is calculated by a sigmoidal function that reduces ingestion rates between salinities of 3 and 10 and suspends ingestion under 3 (threshold values identified from previous literature: Galtsoff 1964, Soniat et al. 2013, and Casas et al. 2018). The DEB model used in the present study used this correction factor to incorporate salinity effects on oyster growth and reproduction.

Table 1: Equations used in the *C. virginica* dynamic energy budget (DEB) model. Adapted from Bernard et al. 2011.

	Equation	Term	Term definition
1	$f = \frac{X}{X + X_k}$	f	Scaled functional response
		X	Food density
		X_k	Half-saturation constant
2	$C_S = \begin{cases} 1, at\ S \geq S_H \\ \frac{S - S_L}{S_H - S_L}, at\ S_L < S < S_H \\ 0, at\ S \leq S_L \end{cases}$	Cs	Salinity correction factor
		S	Salinity
		S_L	Lower salinity threshold
		S_H	Upper salinity threshold
3	$C_T = exp\left\{\frac{T_A}{T_1} - \frac{T_A}{T}\right\}\left(1 + exp\left\{\frac{T_{AL}}{T_1} - \frac{T_{AL}}{T_L}\right\} + exp\left\{\frac{T_{AH}}{T_H} - \frac{T_{AH}}{T_1}\right\}\right)\left(1 + exp\left\{\frac{T_{AL}}{T} - \frac{T_{AL}}{T_L}\right\} + exp\left\{\frac{T_{AH}}{T_H} - \frac{T_{AH}}{T}\right\}\right)^{-1}$	C_T	Temperature correction factor
		T_A	Arrhenius temperature
		T_1	Reference temperature
		T_L	Lower boundary tolerance range

		T_H	Upper boundary tolerance range
		T_{AL}	Arrhenius temperature for lower boundary
		T_{AH}	Arrhenius temperature for upper boundary
4	$\dot{p}_A = C_T\, C_S\, C_{DO}\, \kappa_A\, \{\dot{p}_{Am}\}\, f\, V^{2/3}$	$\dot{p}_A$	Assimilation rate
		C_{DO}	Oxygen correction factor
		κ_A	Assimilation efficiency
		$\{\dot{p}_{Am}\}$	Maximum surface area specific assimilation rate
		V	Structural volume
5	$\dot{p}_{C1} = C_{DO}\left([E]\left(\frac{C_T[E_G]\dot{v}V^{2/3} + C_T\, \dot{p}_M}{[E_G] + \kappa[E]}\right)\right)$	$\dot{p}_{C1}$	Mobilization rate of reserve energy
		$\dot{v}$	Energy conductance
		κ	Fraction of utilized energy to somatic maintenance and growth
		$[E_G]$	Volume-specific costs for structure
		$\dot{p}_M$	Maintenance rate
7	$\dot{p_G} = \kappa \dot{p_{C1}} - \dot{p_{M1}}$	$\dot{p_G}$	Structural growth rate
8	$\dot{p}_{M1} = ([\dot{p}_M]V)C_T$	$[\dot{p}_M]$	Volume-specific maintenance costs
9	$\dot{p}_J = \min(V, V_P)[\dot{p}_M]\left(\frac{1-\kappa}{\kappa}\right)C_T$	$\dot{p}_J$	Maturity maintenance rate
		V_p	Volume at puberty
10	$\dot{p_R} = (1-\kappa)\dot{p}_{C1} - \dot{p}_J$	$\dot{p_R}$	Maturation and reproduction rate
11	$\dot{p}_{L1} = \max(\dot{p}_{M1} - (\kappa\, \dot{p}_{C1} + \dot{p}_{M2} + \dot{p}_{L2}), 0)$	$\dot{p}_{L1}$	Lysis of structure rate
12	$\dot{p}_{C2} = E_R\left(\frac{\{\dot{p}_{Am}\}\kappa_A C_T}{[E_m]V^{1/3}} + \frac{[\dot{p}_M]C_T}{[E_G]}\right)\left(\{1-\kappa\}\frac{E}{[E_G]V + \kappa E}\right)$ If $V \geq V_p$, otherwise 0	$\dot{p}_{C2}$	Gamete mobilization rate
		$[E_m]$	Maximum storage density
13	$\dot{p}_{M2} = \min(\dot{p}_{M1} - \kappa\dot{p}_{C1}, \dot{p}_{C2})$	$\dot{p}_{M2}$	Emergency maintenance rate
14	$\dot{p}_{GO} = \dot{p}_{C2} - \dot{p}_{M2}$	$\dot{p}_{GO}$	Gonad allocation rate
15	$p_{L2} = max\left(\frac{\dot{p}_{M1} - \kappa\dot{p}_{C1} + \dot{p}_{M2}}{Y_{GO}}, 0\right)$	p_{L2}	Gamete resorption rate
		Y_{GO}	Yield of gonad tissue used for maintenance
16	$L = \frac{V^{1/3}}{\delta_V}$	L	Oyster length
		δ_V	Shape coefficient
17			
17	$DD = d(T - T_G)$	DD	Degree-days

		T_G	Threshold temperature for gametogenesis
	Differential Equations		
18	$\frac{dE}{dt} = \dot{p}_A - \dot{p}_{C1}$		Reserves
19	$\frac{dV}{dt} = \left(\frac{\dot{p}_G - \dot{p}_{L1}}{[E_G]}\right)$		Structural volume
20	$\frac{dE_R}{dt} = \dot{p}_R - \dot{p}_{C2}$		Reproduction
21	$\frac{dE_{GO}}{dt} = \dot{p}_{GO} - \dot{p}_{L2}$		Gametes

173 Table 2: State variables and parameters used in the *C. virginica* DEB model.
174

State Variable	**Symbol**		**Unit**	
Structural volume	V		cm^3	
Reserve energy	E		J	
Reproduction energy	E_R		J	
Gonad energy	E_{GO}		J	
Parameter	**Symbol**	**Value**	**Unit**	**Source**
Half-saturation constant	X_k	1.5	μg chl l^{-1}	Lavaud et al. 2017
Shape coefficient	δ_V	0.24884	--	Powell et al. 1995, Lavaud et al. 2017
Maximum surface area-specific ingestion rate	$\{\dot{p}_{Xm}\}$	249.5	J cm^{-2} d^{-1}	Lavaud et al. 2017
Surface area-specific maximum assimilation rate	$\{\dot{p}_{Am}\}$	187	J cm^{-2} d^{-1}	$\{\dot{p}_{Xm}\}*\kappa_A$
Assimilation efficiency	κ_A	0.75	--	Gerdes 1983, Lavaud et al. 2017
Fraction of reproduction buffer fixed into eggs	κ_R	0.95	--	Lavaud et al. 2021
Allocation fraction	κ	0.82	--	Lavaud et al. 2017
Yield of gonad tissue used for maintenance	Y_{GO}	0.25	--	Bernard et al. 2011
Volume-specific somatic maintenance costs	$[\dot{p}_M]$	38	J cm^{-3} d^{-1}	Lavaud et al. 2017
Volume-specific cost for structural growth	$[E_G]$	5230	J cm^{-3}	Lavaud et al. 2017
Maximum reserve density	$[E_m]$	5420	J cm^{-3}	Lavaud et al. 2017
Maturity threshold at puberty	E_H^p	370	J	Lavaud et al. 2017
GSI threshold for spawning	GSI	30	-	Barber et al. 1991
Spawning efficiency	k_{sp}	1	-	Kennedy and Krantz 1982
Energy conductance	$\dot{v}$	0.03453	cm d^{-1}	Lavaud et al. 2017
Maturity maintenance rate coefficient	$\dot{k}_J$	0.002	d^{-1}	Lavaud et al. 2017
Salinity Function				
Upper salinity threshold	S_H	10	ppt	Lavaud et al. 2017
Lower salinity threshold	S_L	3	ppt	Lavaud et al. 2017
Temperature function				
Arrhenius temperature	T_A	6700	K	Lavaud et al. 2017
Reference temperature	T_1	293.15	K	--
Lower boundary tolerance range	T_L	283.15	K	Galtsoff 1964
Upper boundary tolerance range	T_H	303	K	Galtsoff 1964
Arrhenius temperature for lower boundary	T_{AL}	21820	K	Lavaud et al. 2017
Arrhenius temperature for upper boundary	T_{AH}	45380	K	Lavaud et al. 2017
Temperature threshold for gametogenesis	T_G	12	°C	Price and Mauer 1971
Temperature threshold for spawning	T_{sp}	20	°C	Shumway 1996
Additional and compound parameters	**Symbol**	**Value**	**Unit**	**Source**

Structure density	d_V	0.2	$g_{DW}\ g_{WW}^{-1}$	Lavaud et al. 2017
Chemical potential of structure	μ_V	15600	$J\ g^{-1}$	Bernard et al. 2011
Chemical potential of reserve	μ_E	19600	$J\ g^{-1}$	Bernard et al. 2011
Dry weight to wet weight ratio	*dw:ww*	0.2	--	Lavaud et al. 2017
Egg energy	ρ_{egg}	$2.566\ 10^{-4}$	$J\ g^{-1}$	Lavaud et al. 2021
Dry mass of egg	W_{egg}	$4\ 10^{-8}$	$g\ egg^{-1}$	Lavaud et al. 2021

175

Gametogenesis and spawning activities vary between species and have been modeled in several different ways in DEB models developed for bivalves (e.g., Lavaud et al. 2014, Pouvreau et al. 2006, Bernard et al. 2011). *C. virginica* is known to undergo gametogenesis once they've reached a threshold size (volume at puberty [V_P]) and ambient temperatures rise above a threshold gametogenesis temperature (T_G) (Price and Mauer 1971). Spawning is triggered after an accrual of degree-days above T_G, ambient temperatures have reached the spawning temperature (T_{sp}) (Shumway 1996), and an individual has grown to attain a threshold gonado-somatic index (GSI) (Choi 1992), measured by:

$$GSI = \frac{GDW}{TDW} \times 100 \quad (1)$$

where GDW is equal to the gonad dry mass and TDW denotes the total dry tissue mass. In the present model, gametogenesis occurred only when oysters were above the previously parameterized volume at maturity (0.416 cm^3, Lavaud and Kooijman 2018) and temperatures exceeded 12°C (Price and Mauer 1971). Spawning was triggered when oysters reached a threshold GSI of 30% (Barber et al. 1991), 434 degree-days above 12°C had accrued (Mann et al. 2014), and ambient temperatures were above 20°C (Shumway 1996). The gonads were completely emptied upon spawning (Kennedy and Krantz 1982). An accurate estimate of spawning GSI for Chesapeake Bay oysters was not available for use in the current model. The GSI threshold of 30% used for this study was determined based off of a gonadal area index from a study of oyster reproduction in nearby Delaware Bay (Barber et al. 1991). In contrast to GSI – measured as the ratio of gonad dry weight to total dry tissue weight – gonadal area index is measured as a ratio of gonadal area to the entire visceral mass. While not an exact measure of

GSI, the use of this value in the model produced estimated spawning patterns that were consistent with the timing and frequency of spawns observed in oysters from the Chesapeake Bay (Mann et al. 2014).

2.2 Oxygen Correction Function

A primary goal of the present study was to incorporate dissolved oxygen as an additional forcing variable into the *C. virginica* DEB model. Similar to previous work (Aguirre-Velarde et al. 2019a, Lavaud et al. 2019), this was accomplished through the integration of an oxygen correction factor (C_{DO}) to constrain energy fluxes in the DEB model. To parameterize C_{DO}, a consideration of *C. virginica*'s response to declining oxygen tension is necessary. *C. virginica* is known to elicit a two-phase response in oxygen consumption across declining oxygen tensions, where oxygen consumption rates are maintained above a threshold oxygen concentration and decline linearly as concentrations fall below the threshold (Shumway and Koehn 1982). Thus, similar to Aguirre-Velarde et al. (2019a), C_{DO} in the present study was modeled using a two-phase response using the following equation:

$$\text{for } C_{O2} < C_{O2c}, \; C_{DO} = \frac{C_{O2}}{C_{O2c}} \text{, else } 1 \qquad (2)$$

where C_{O2} is the dissolved oxygen concentration at any given point and C_{O2c} denotes the threshold (or critical) oxygen concentration.

Critical oxygen concentrations (also identified as P_{crit}) vary considerably both interspecifically (Vaquer-Sunyer and Duarte 2008) as well as intraspecifically, either as a result of differential

tolerance to low oxygen (e.g., Sollid et al. 2003) or as a result of the ambient environmental conditions during which it's measured (Rogers et al. 2016). With respect to *C. virginica*, oxygen uptake measured across a range of dissolved oxygen concentrations has been shown to differ depending on the ambient temperature and salinity (Shumway and Koehn 1982). Since temperature and salinity also force the DEB model, a dynamic C_{O2c} equation was parameterized to integrate their effect on the critical oxygen concentration. To accomplish this, critical oxygen concentrations were extrapolated from the oxygen uptake curves measured across three temperatures and three salinities from Shumway and Koehn (1982) by identifying the dissolved oxygen concentration at which oxygen uptake began to decline. Then, a linear model relating salinity and temperature to the critical oxygen concentration was determined using the *lm* function in R (Figure 2). The resulting equation:

$$C_{O2c} = 0.00148\,T[t] - 0.173\,S[t] + 7.0756 \quad (3)$$

was used to vary the critical oxygen concentration depending on the ambient temperature (T) and salinity (S) at a given time point (t).

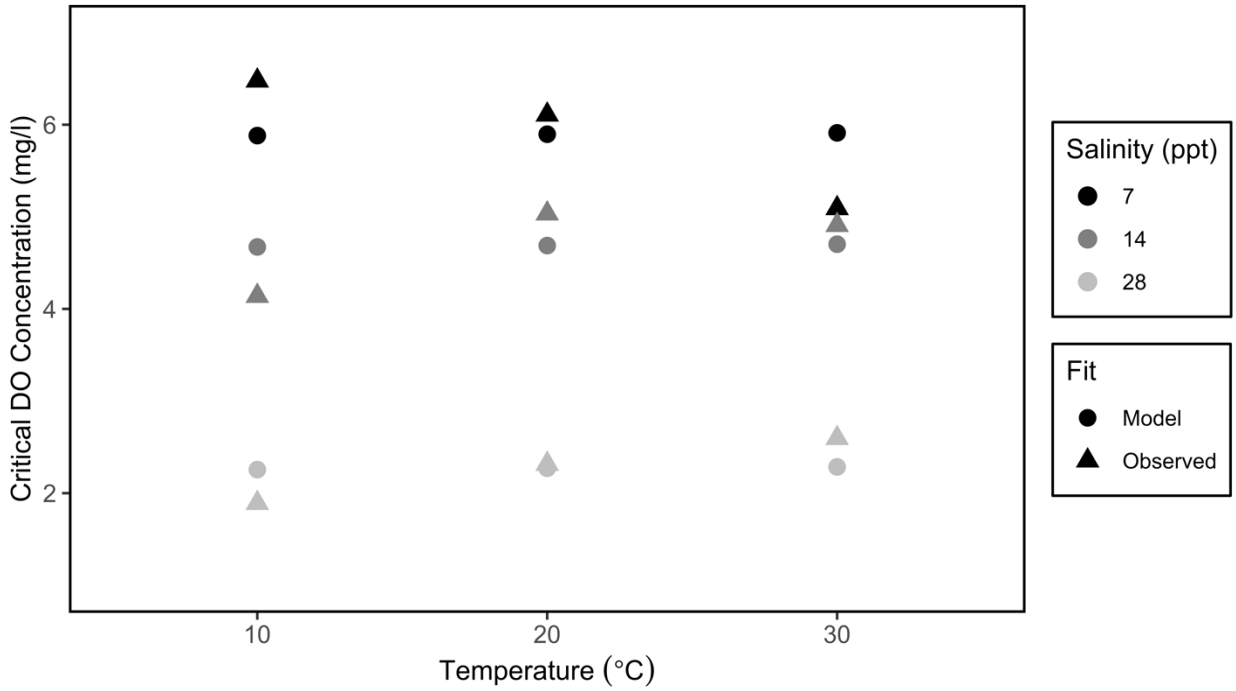

Figure 2: Comparison of observed critical oxygen concentrations across three temperatures and three salinities from Shumway and Koehn (1982) versus the predicted values from the linear model (Equation 3).

Oxygen correction factors have previously been used in DEB models to constrain ingestion rates for cod (Lavaud et al. 2019) or assimilation and mobilization rates for scallops (Aguirre-Velarde et al. 2019a). While prior work using the oxygen correction factor for bivalves did not include an effect of oxygen on feeding, oysters have been shown to reduce their ingestion rates during low oxygen stress (Clark 2014). Thus, in addition to effects of dissolved oxygen on assimilation ($\dot{p}_A$), and mobilization ($\dot{p}_C$) rates, the present study also applied C_{DO} to constrain ingestion rates ($\dot{p}_X$) of the oysters as follows (parameter definitions are listed in Table 2):

$$\dot{p}_X = C_T C_{DO} C_S \{\dot{p}_{Am}\} f V^{2/3}$$

$$\dot{p}_A = C_{DO}\, \dot{p}_X k_A \quad (4)$$

256 $$\dot{p}_C = C_T C_{DO} \left(\frac{[E]}{[E_G] + \kappa[E]} \, \dot{v} \, [E_G] V^{2/3} + \dot{p}_M \right)$$

257

258 The result is a two-phase response to oxygen availability. When oxygen concentrations are above
259 the critical oxygen concentration ingestion, assimilation, or mobilization rates of the oyster are
260 not affected by oxygen availability. Below the critical oxygen concentration, the oxygen
261 correction factor declines linearly between 1 and 0, leading to a reduction in the ingestion,
262 assimilation, and mobilization rates.

263

264 To assess the assumptions presented above and how their integration into the model affected the
265 model fit, six independent models were run on environmental datasets for oysters from two of
266 the validation sites, Chesapeake Biological Lab and Cole's Creek (see *Model Validation* below)
267 and their fit to the observed oyster growth data was assessed. The first model ('No oxygen
268 effect') was run using the standard DEB model – including the salinity correction factor –
269 without any effect of dissolved oxygen to determine how the model fit the data without an
270 integration of C_{DO}. The second model ('Static C_{O2c}') included an effect of oxygen on
271 assimilation ($\dot{p}_A$), mobilization ($\dot{p}_C$), and ingestion ($\dot{p}_X$) rates, with a static critical oxygen
272 concentration set at 2.0 mg/l, the level used to broadly define 'hypoxia' (Rabalais et al. 2010).
273 This model was intended to assess how integration of a C_{DO} into the model without a
274 consideration of the interactions between dissolved oxygen and other environmental forcing
275 variables predicted oyster growth data. The third model ('Assimilation') incorporated the
276 dynamic C_{O2c} to calculate the C_{DO}, but only acted on assimilation rates, whereas the fourth
277 model ('Mobilization') included a dynamic C_{O2c} only acting on mobilization rates. The fifth
278 model ('Assimilation + Mobilization') replicated the DEB model by Aguirre-Velarde et al.

(2019a) by applying the C_{DO} to both the assimilation and mobilization rates. The sixth and final model ('Full Model') used a dynamic C_{O2c} to calculate the C_{DO}, which was then applied to the ingestion, assimilation, and mobilization rates. The fit of these models was assessed by calculating the root-mean square error (RMSE) between the observed and simulated oyster shell lengths.

2.3 Oyster Growth and Environmental Data

Oyster growth data used in model validation was collected in 2008 and 2009 as part of a study conducted by Breitburg et al. (2015) examining the susceptibility of oysters to *Perkinsus marinus* (Dermo) infection in relation to low-oxygen exposure. The reader is referred to this study for a detailed description of the experimental setup. Briefly, oysters were deployed suspended in polyethylene mesh cages at sites throughout tributaries of the Chesapeake Bay. Water quality parameters – temperature (°C), salinity, dissolved oxygen (mg/l), and chlorophyll-*a* (μg/l) – were continuously monitored at 15-minute intervals at each site using Yellow Springs Instruments model 6600 sondes (Yellow Springs Instruments, Yellow Springs, OH). In June of each year, initial oyster shell lengths to the nearest millimeter were measured prior to the deployment of the oysters in the field. Final shell lengths were measured when oysters were retrieved in early October. In 2008, three intermediary shell length measurements – each approximately one month apart – were taken on a subsample of deployed oysters, while only one midpoint measurement on a subsample of oysters was taken in 2009. Numbers of oysters measured at each site and time point are shown in Supplementary Table 1. Shell lengths for all oysters were measured with a flexible ruler wrapped across the longest dimension from hinge to the tip of the valve to account for three-dimensional growth of the shell. A subset of oyster shell lengths was also measured

with calipers along the same shell axis. Data were collected on both one- and two-year-old oysters, although only growth of one-year-old oysters were used for the model validation in the present study in order to maintain consistency of oyster age across sites.

Two modifications were made to the oyster growth and environmental data prior to their use in modeling. First, since the DEB model output of shell length does not account for the three-dimensional curvature of the shell, it was necessary to transform the three-dimensional flexible ruler measurement to the two-dimensional caliper measurement for comparison with the model. To do so, a power function was fit to the data relating the flexible ruler and caliper measurements (Supplementary Figure 1) and resulting equation ($Caliper\ Length = 1.1879\ Ruler\ Length^{0.9383}$) was used to transform the three-dimensional lengths to two-dimensional lengths. Second, the continuous water quality monitoring data from the validation sites contained some gaps in data measurements, which were necessary to rectify prior to use in the model. These missing data points were interpolated using the MATLAB (version 9.10.0.1602886 R2021a) *fillgaps* function, which uses autoregressive modeling to interpolate the data. The data were interpolated using 24 data points (six hours) worth of data from either side of the gap, which visually provided the best fit of the interpolated data to the trends of the measured data. Statistics for the number of interpolated datapoints for each environmental dataset is provided in Supplementary Table 2.

2.4 Model Validation

The model was validated against empirically measured oyster growth data from eight different sites, four generally normoxic sites in the Chesapeake Bay (Chesapeake Biological Lab [CBL],

Bowler's Wharf [BWH], Mulberry Point [MUL], and Yeocomico River [YEO]) and three reduced oxygen sites (Cole's Creek [CCR], Harness Creek [HCR], Little Monie Creek [LMN], and St. Mary's College [SMC]) (Figure 3). The four normoxic sites all had dissolved oxygen measurements above 2.0 mg/l, whereas the three hypoxic sites had 2.7% (CCR), 3.1% (HCR), 0.1% (LMN), and 12.2% (SMC) of dissolved oxygen measurements below 2.0 mg/l (Supplementary Figures 2-9).

Model validation was run using the model with the dynamic C_{O2c} acting on ingestion, assimilation, and mobilization rates ('Full Model' as described above). For each site, the initial shell length (L_0) for the model run was set to the mean starting shell length from the oyster growth dataset and this value was used to calculate the initial total energy (*TE*) in an individual according to the equation (McFarland 2015):

$$TE = \frac{\{\dot{p}_{AM}\}}{\dot{v}} (L_0\, \delta_M)^3 \quad (5)$$

where $\{\dot{p}_{AM}\}$ is equal to the maximum surface area-specific assimilation rate, $\dot{v}$ is equal to the energy conductance, and δ_M is equal to the shape coefficient. Simulations began in mid-June, just as oysters would have been preparing to spawn in the Chesapeake Bay (Thompson et al. 1996). Empirical measures of energy allocation towards reserves (E), reproductive buffer (E_R), and gonad energy (E_{GO}) were not available to set initial values for the model. Thus, the initial percentage of energy in reserves was estimated at 70%, with the remaining energy allocated towards energy in the reproductive buffer at 20% and gonad energy at 10%, following a similar allocation of energy as estimated by Filgueira et al. (2014) for summertime oysters.

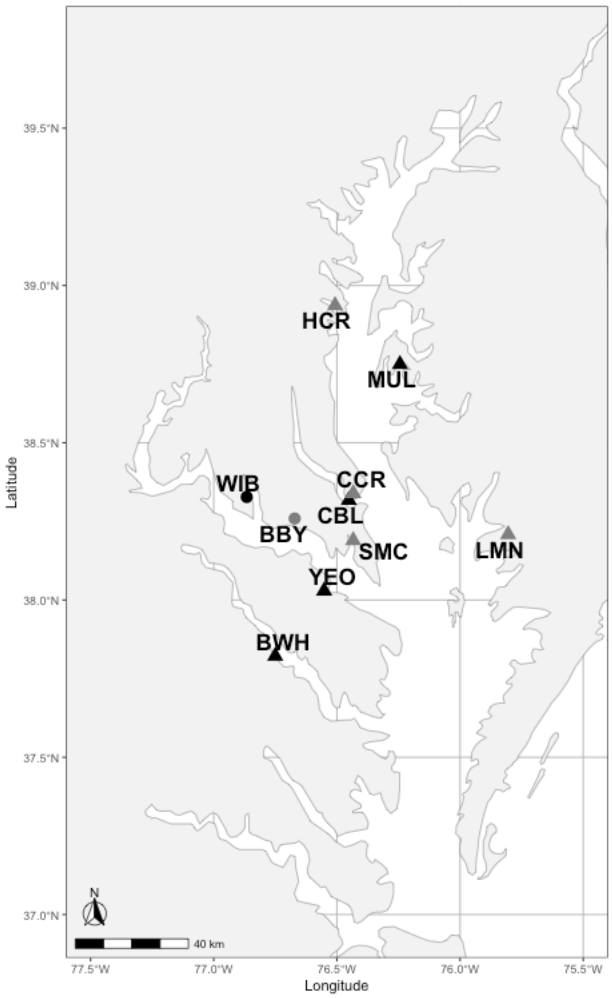

Figure 3: Map of Chesapeake Bay, USA with the sites used in the modeling analyses. Low oxygen sites are denoted by grey markers and normoxic sites are denoted by black markers. Validation sites (▲), Chesapeake Biological Lab (CBL), Cole's Creek (CCR), Harness Creek (HCR), Bowler's Wharf, Rappahannock River (BWH), Little Monie Creek (LMN), Mulberry Point (MUL), St. Mary's College (SMC), and Yeocomico River (YEO). Prediction sites (●), Breton Bay (BBY) and Wicomico Beach (WIB).

The fit of the simulated oyster shell lengths to the observed shell lengths was assessed in two ways. First, a linear model was run on the simulated and observed oyster shell lengths. The resulting slope and intercept of the equation was used to determine how close the model fit to a 1:1 relationship between observed and simulated shell lengths, while the R^2 value was used to

363 determine the amount of variance in the simulated shell lengths explained by the variance in the
364 observed shell lengths. Second, deviations (F) between the simulated (L_S) and observed (L_0)
365 shell lengths were calculated according to Rosland et al. (2009):
366
367 $$F = \frac{100}{2T}\left(\sum_{t=1}^{T}\frac{|L_S(t) - L_O(t)|}{L_O(t)}\right) \quad (6)$$
368
369 where T is the total number of shell length comparisons made for each site for each given time
370 point (t). Smaller values of F would correspond to a better fit between observed and simulated
371 oyster shell lengths.
372
373 *2.5 Predicting Oyster Growth and Reproduction*
374 The validated model was used to make predictions about oyster growth and reproductive output
375 over the full growing season for oysters at two sites that differ in oxygen availability, Wicomico
376 Beach (WIB) and Breton Bay (BBY) both in the Potomac River, Maryland (Figure 2).
377 Continuous monitoring data for temperature, salinity, chlorophyll-*a* concentration, and dissolved
378 oxygen concentration were downloaded from Maryland Department of Natural Resources Eyes
379 on the Bay (http://eyesonthebay.dnr.maryland.gov [last accessed September 6, 2023]) for each of
380 the sites from April through October 2007, the duration of time the water quality monitoring
381 sondes were deployed (Supplementary Figure 10). Missing datapoints for the water quality data
382 were interpolated using identical methods to the model validation environmental data described
383 above. Initial shell length for each model run was set to 4.5 cm, an approximate length for one-
384 year-old oysters in the Chesapeake Bay (Coakley 2004). Oysters used in the prediction analyses
385 were predicted to have less energy in their gonads than those used in the validation datasets since

oysters typically overwinter with very little energy stored in gonads (Thompson et al. 1996) and gametogenesis typically would begin after the beginning of the model run (April or May according to Kennedy and Krantz 1982). Thus, initial values for energy allocation were slightly altered from the validation model runs, with 0.7 of total energy in reserves (E) and 0.3 of total energy in reproduction (E_R). No energy was predicted to be in the gonads (E_{GO}) and initial degree-days were set to zero since water temperatures in the Chesapeake Bay before April are typically not above 12°C, the gametogenesis temperature threshold (NOAA National Data Buoy Center [https://www.ndbc.noaa.gov] last accessed September 6, 2023). The model was used to predict overall shell length, total wet tissue mass, and gonad wet mass at each of the sites. Shell (cm/month) and wet tissue mass (g/month) growth rates (*GR*) were calculated according to the following equation:

$$GR = \frac{M_E - M_0}{7} \quad (7)$$

where M_E and M_0 denote the ending and initial size measurements, respectively, and seven corresponds to the number of months the model was run. Additionally, resulting gonad wet mass was used to assess timing of spawning and fecundity of spawning oysters (number of eggs spawned) using the equation:

$$Number\ of\ eggs = \frac{E_{sp}}{\rho_{egg}} \quad (8)$$

where E_{sp} is the energy released during spawning and ρ_{egg} is the amount of energy in a single egg. In the case of multiple spawnings, the number of eggs was totaled across the whole season.

3. Results

3.1 Oxygen Correction Factor

Results of the alternative model comparisons for integrating dissolved oxygen into the DEB model indicated that including the effects of dissolved oxygen on oyster growth, specifically by using a dynamic C_{O2c} provided the greatest improvement of model fit for both sites, but particularly CCR, the site experiencing low oxygen conditions (Table 3). Overall, the best model fit for both sites was for the 'Full Model' that integrated a dynamic C_{O2c} acting on assimilation, mobilization, and ingestion rates to determine C_{DO} (RMSE: CBL=0.357, CCR=0.600) while the worst model fit included no effect of dissolved oxygen on oyster growth (RMSE: CBL=0.418, CCR=0.995).

Table 3: Root-mean square error between observed and predicted oyster shell lengths for the six tested alternative models of dissolved oxygen integration. Models were run on two of the validation sites, Chesapeake Biological Lab (CBL) and Cole's Creek (CCR). 'Full Model' describes the model that incorporated a dynamic C_{O2c} acting on assimilation, mobilization, and ingestion rates.

	Site	
	CBL	**CCR**
No oxygen effect	0.418	0.995
Static C_{O2c}	0.418	0.968
Assimilation	0.395	0.820
Mobilization	0.399	0.843
Assimilation + Mobilization	0.377	0.698
Full Model	0.357	0.600

Table 4: Deviations (*F*, %) between observed and simulated shell lengths for the sites used in model validation. Values calculated using Equation 7.

Site	F
Normoxic	
BWH	5.934
CBL	3.053
MUL	2.040
YEO	7.788
All normoxic sites	4.704
Hypoxic	
CCR	3.887
HCR	5.212
LMN	5.859
SMC	3.812
All hypoxic sites	4.693
All Sites	4.698

3.2 Model Validation

The model was validated against eight different observed oyster growth datasets and there was strong agreement between simulated and observed shell lengths at each site (Figure 4). The empirical growth data indicated that oysters from the sites with low oxygen exposure grew by a smaller percent change in shell length (CCR 22.7%, HCR 23.3%, LMN 23.0%, SMC 15.5%) compared to the normoxic site oysters (BWH 29.2%, CBL 29.1%, MUL 32.0%, YEO 23.2%), and the model was able to predict these changes in length fairly well (Model predictions - Low oxygen: CCR 21.7%; HCR 24.0%, LMN 16.9%, SMC 17.3%; Normoxic: CBL 24.9%, BWH 24.4%, MUL 30.2%, YEO 26.4%). The linear model assessing the fit of the simulated oyster growth in shell length compared to the observed growth showed a nearly 1:1 relationship between simulated and observed data (Figure 5; slope=1.17, intercept=0.78, R^2=0.65, $p < 0.001$). Deviations between simulated and observed oyster lengths were also relatively minimal and showed strong agreement between the model and observed data, with an average deviation of 4.70% across all sites (Table 4). One site, Yeocomico River (YEO), showed the largest deviation

of 7.79%, where the model tended to overestimate the growth of oysters, particularly at the midpoint measurement (Figure 4G).

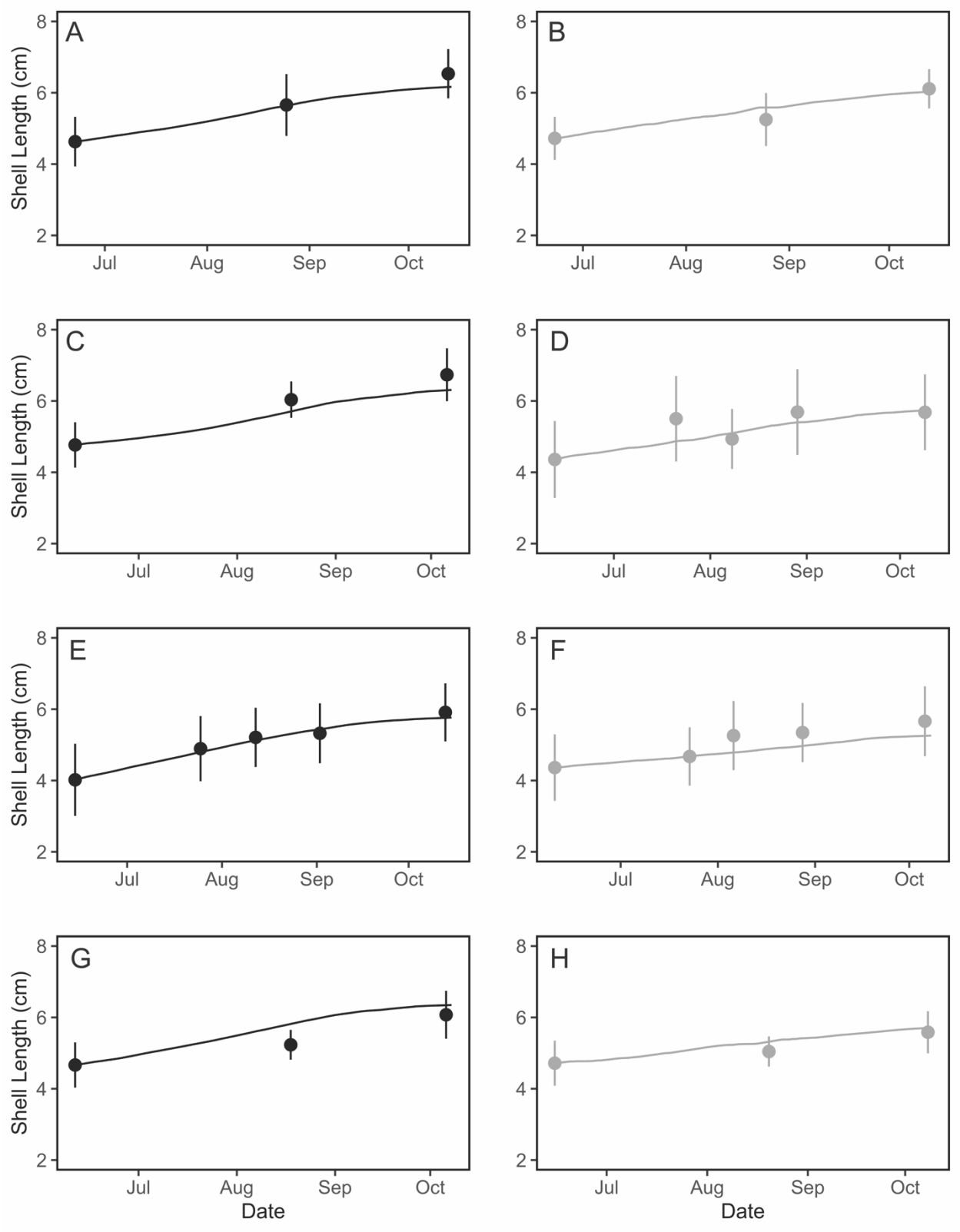

Figure 4: Oyster shell length (cm) growth for sites used in model validation. Normoxic sites CBL (A), BWH (C), MUL (E), and YEO (G) are shown in black and low oxygen sites CCR (B), HCR

(D), LMN (E), and SMC (H) are shown in grey. Lines denote predicted growth from model. Mean observed oyster sizes are shown as points and error bars denote standard deviation. Sample sizes of oysters measured at each timepoint at each site are specified in Supplementary Table 1.

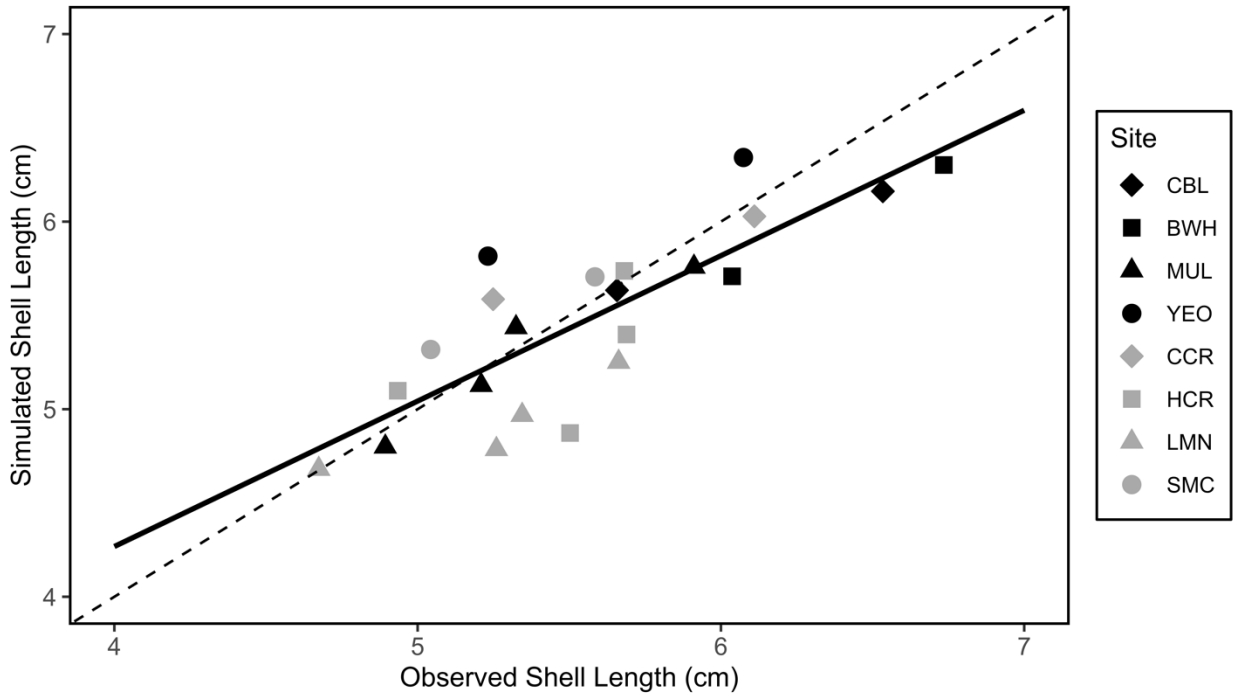

Figure 5: Observed versus simulated shell lengths for the six sites used in model validation. Initial lengths are not included as the initial oyster length for the model runs were averaged from the observed shell lengths. Black markers represent normoxic sites and grey markers represent low oxygen sites. The dashed line denotes a 1:1 relationship between the modeled and observed shell lengths. The solid line corresponds to the linear regression line relating observed and simulated values (slope=1.17, intercept=0.78, R^2=0.65, $p < 0.001$).

3.3 Predicting the Effects of Low Oxygen on Oyster Growth and Reproduction

The model predicted overall greater growth in both oyster shell length and whole tissue weight, as well as greater reproductive output for the oysters from the normoxic site, Wicomico Beach

(WIB) compared to the low oxygen site, Breton Bay (BBY) (Figure 6). The final predicted oyster shell length for WIB was 6.45 cm, with an average growth rate of 0.28 cm/month. The final oyster shell length for BBY was 6.01 cm, with an average growth rate of 0.22 cm/month. Oysters from WIB were approximately 7.4% longer than oysters from BBY (Figure 6A). Final whole wet tissue weight showed a larger difference between the two sites, with BBY predicted to have approximately 24.6% less weight in their tissues at the conclusion of the model run. The

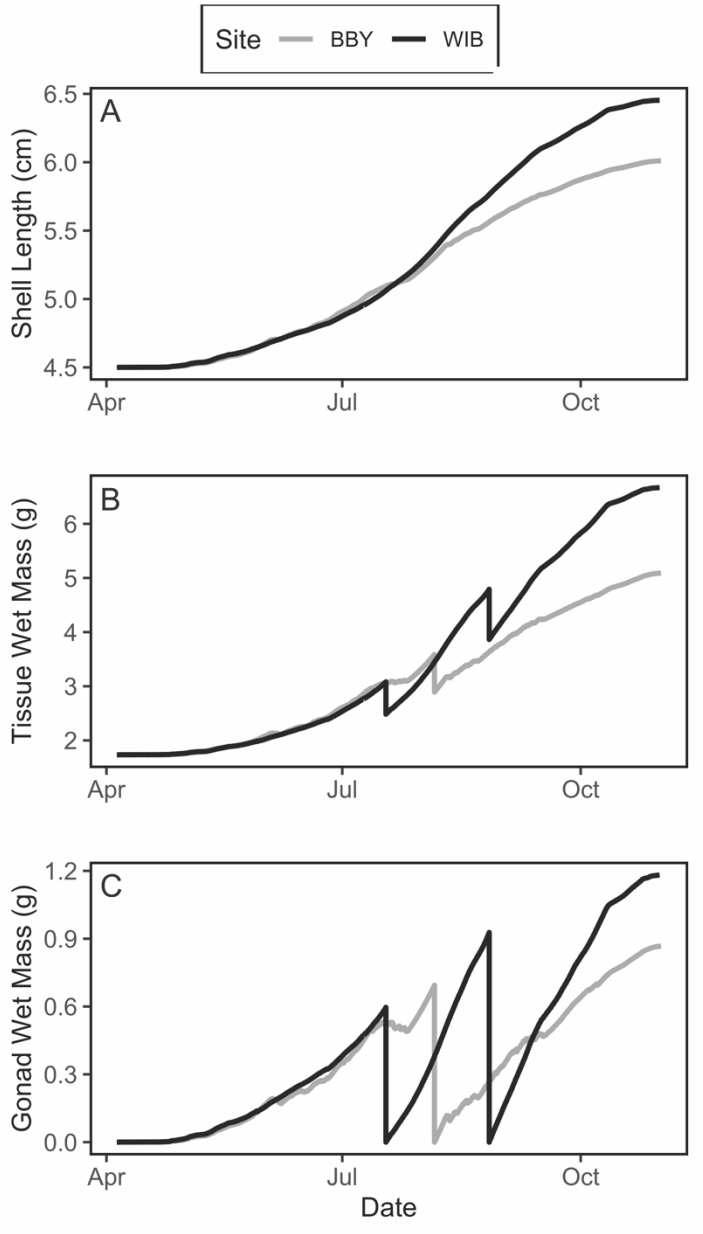

Figure 6: Predicted A) shell length, B) tissue wet mass, and C) gonad wet mass for Wicomico Beach (WIB; normoxic site) and Breton Bay (BBY; low oxygen site).

final wet tissue mass of WIB oysters was 6.67 g and the final wet tissue mass of BBY oysters was 5.09 g, with growth rates of 0.70 g/month and 0.48 g/month respectively (Figure 6B). Reproductive output also differed between sites (Figure 6C). Oysters from the hypoxic site were predicted to reproduce one time throughout the summer, in early August, whereas oysters from the normoxic site spawned two times, in July and late August. Overall, a 54.4% reduction in fecundity for hypoxic site oysters was predicted, with a total spawning output of approximately 5.4 million eggs throughout the season at the hypoxic site compared to a total spawning output of approximately 11.8 million eggs at the normoxic site.

4. Discussion

Mechanistic modeling, such as the Dynamic Energy Budget (DEB) model, provides a useful tool to make predictions about the effects of environmental stressors on organismal growth and reproduction. Hypoxia is a pervasive oceanic and coastal stressor that is predicted to increase in frequency in marine environments into the future (Breitburg et al. 2018). Given the importance of oxygen availability for aerobic respiration, the integration of oxygen availability into individual bioenergetics models can provide an important step in scaling individual effects of low oxygen onto broader population dynamics. The present study provides a first step in the integration of dissolved oxygen into the DEB model for *C. virginica*. The incorporation of an oxygen correction factor on aspects of oyster energetic flux improved the fit of the model for oyster shell growth, particularly for oysters in low oxygen habitats. The model predicted empirically measured Chesapeake Bay oyster growth data well using previously published

parameters for *C. virginica,* indicating that the oyster DEB model is well-parameterized for this species. Importantly, preliminary predictions from the model of oyster growth and reproductive output at two different sites in the Chesapeake Bay indicate that reduced oxygen availability decreases oyster's overall growth and fecundity and alters the frequency and timing at which an oyster spawns during the summer.

4.1 Integration of Dissolved Oxygen as a Forcing Variable

A primary goal of the present study was the integration of dissolved oxygen into the DEB growth model for adult *C. virginica*. Oxygen is necessary for energy production in aerobically-respiring organisms and is therefore predicted to be an important abiotic force driving organismal bioenergetics (Thomas et al. 2019). Prior studies parameterizing the integration of dissolved oxygen into DEB models have used oxygen correction factors to constrain energetic fluxes within the model and have shown improved prediction of organismal growth in low oxygen habitats (Aguirre-Velarde et al. 2019a, Lavaud et al. 2019). By using a similar oxygen correction factor within the *C. virginica* DEB model, the model used in the present study was able to accurately estimate differences in oyster growth between sites with differing oxygen availability (Figure 4). Two modifications were made to the prior integration of C_{DO}. First, a dynamic (as opposed to static) critical oxygen concentration (C_{O2c}) was used to calculate C_{DO}, as prior work indicates this value varies as a result of the other DEB model forcing variables, temperature and salinity (Shumway and Koehn 1982). The integration of a dynamic value led to an improvement in model fit for the oysters from the hypoxic site, CCR (Table 3). The effect of ambient temperature and salinity on the ability of marine organisms to regulate their oxygen consumption is true for many organisms beyond *C. virginica* (Herreid 1980, Rogers et al. 2016). Thus, for

future integration of a C_{DO} term into DEB models, particularly for marine ectotherms, the use of a dynamic critical oxygen concentration is of great importance. Second, the model used an additional constraint on ingestion rates for *C. virginica*, compared to prior work with bivalves where C_{DO} acted only on energy assimilation and mobilization rates (Aguirre-Velarde et al. 2019a). Given the close link between oyster feeding and respiration, lowered oxygen availability reduces oyster ingestion rates (Clark 2014). For oysters from the low oxygen site, the additional constraint on ingestion rates further improved model fit (Table 3).

Validation of the model against eight different sites in the Chesapeake Bay indicated that the simulated oyster growth fit the observed data well, with a nearly 1:1 relationship and very small deviations between the observed and simulated shell lengths, regardless of the oxygen conditions of the site (Figure 5). The model slightly overestimated growth for oysters from one normoxic site, Yeocomico River (YEO), compared to the other validation sites (Figure 4). This was reflected in the fact that the deviation between the simulated and observed shell lengths for YEO (F=7.788%) was the largest for all of the sites (Table 4). There are two plausible explanations for the observed difference in fit. First, the higher deviation could have been the result of random chance in oyster sampling during measurement. The estimated oyster length for the intermediate measurement of oysters at YEO was outside of the standard deviation of observed lengths (Figure 4G) and thus likely drove the higher deviation for this site. Because the length measurements for the intermediate timepoints were reliant on a small, haphazardly collected subsample of oysters (18 individuals oysters out of the 120 oysters deployed at YEO), it's possible that the smaller shell length of the collected oysters at this timepoint could have simply been due to a random sample consisting of smaller oysters. Second, it is also possible that

another unmodeled environmental factor was acting on the oysters from this particular site. The focus of the study from which the oyster growth data was collected was examining susceptibility of oysters to the parasitic disease *Perkinsus marinus* in relation to hypoxia exposure. Data on infection intensity per site was not reported in Breitburg et al. (2015), but YEO did trend towards a higher mean level of infection intensity with *P. marinus* than the other normoxic sites, BWH and MUL (D. Hondorp, *personal communication*). The reduced growth rate not captured by the model may have therefore been a result of this additional stressor. Regardless of the reason for the reduced fit, the difference between the simulated and observed shell lengths is minimal at YEO and, overall, the model predicted oyster growth well in both site types indicating its utility in predicting oyster growth in varying oxygen conditions.

4.2 Predicted Effects of Hypoxia on Oyster Growth

Environmental water quality data from two sites with differing oxygen regimes in the Chesapeake Bay were used to force the validated model in order to make predictions about how hypoxia exposure during the growing season affects oyster growth and reproduction. One of the primary predictions from the model was that oyster shell growth rates would be reduced for oysters from the low oxygen site (Figure 6A). Predicted growth rates for oysters from the normoxic site, WIB (0.28 cm/month), were higher compared to the low oxygen site, BBY (0.22 cm/month). Overall, the predicted growth rates fall within the range of observed oyster growth rates in the Chesapeake Bay (0.64±0.33 cm/month, Paynter and Burreson 1991; 0.11±0.029 cm/month, Paynter and DiMichele 1990). Additionally, the 21.4% reduction in growth rate between sites is consistent with the approximately 30% reduction in growth rate that has

576 previously been shown for *C. virginica* exposed to chronic hypoxic conditions for four weeks
577 (Stevens and Gobler 2018).
578
579 Reduced growth was also observed in the wet tissue mass for oysters from the low oxygen site
580 compared to the normoxic site (Figure 6B). It should be noted that empirical data on oyster tissue
581 growth was not available for validation of the model for the present study. However, predicted
582 values for wet tissue mass are close to values predicted by an allometric scaling relationship
583 between oyster wet tissue mass and oyster length (Pollack et al. 2011). Using the allometric
584 model to predict oyster wet mass from the DEB model predictions of oyster length, final wet
585 tissue mass for oysters from the normoxic site was calculated at 4.89 g compared to model
586 prediction of 6.67 g for oysters from the normoxic site and calculated at 3.94 g compared to
587 model prediction of 5.09 g for the low oxygen site. It is unknown how well this allometric
588 scaling relationship predicts oyster wet tissue mass throughout the reproductive cycle. While the
589 oyster wet mass predicted by the allometric scaling relationship are comparable to the values
590 produced by the DEB model, additional empirical studies are needed to determine to what extent
591 these model outputs represent effects of low oxygen on oyster tissue mass. Additionally, a
592 greater decrease in final tissue mass (23.6%) compared to oyster shell length (6.9%) was
593 observed for low oxygen site oysters compared to normoxic site oysters, which may indicate a
594 lower fitness of oysters from the low oxygen site. Tissue growth is more energetically costly than
595 shell growth (e.g., Watson et al. 2017), thus a decrease in energy allocated to tissue growth for
596 oysters exposed to low oxygen would indicate the oysters' energetic demands are not being met
597 to produce sufficient tissue growth.
598

599 Overall, the reduced growth in shell length and wet tissue mass predicted for oysters from the
600 low oxygen site have implications for the ecology of oyster reefs in the Chesapeake Bay. Slowed
601 growth rates and smaller size-at-age for oysters exposed to periodic hypoxia could reduce the
602 capacity of oysters to provide ecosystem services, such as water filtration (Zu Ermgassen et al.
603 2013). Additionally, oysters from low oxygen sites may take longer to reach a size refuge and
604 would be more likely to be predated upon since smaller oysters are more prone to predation
605 (Eggleston 1990). While the model does not make predictions about juvenile oyster growth,
606 similar patterns of reduced growth under hypoxic conditions have been shown in juvenile oysters
607 (Baker and Mann 1992), which could delay maturity for oysters.
608
609 *4.3 Predicted Effects of Hypoxia on Oyster Reproduction*
610 In addition to constraints on growth, oysters at hypoxic sites were also predicted to experience
611 adverse reproductive effects as a result of low dissolved oxygen availability during the summer
612 growing season. Overall fecundity for oysters at the reduced oxygen site, BBY, was predicted to
613 be greatly reduced, with 54.4% fewer eggs released each year compared to the normoxic site,
614 WIB. These data align with findings from prior research on bivalve reproductive response to low
615 oxygen as a similar 40% reduction in egg production has been reported in the clam *Macoma*
616 *balthica* due to exposure to hypoxia (Long et al. 2014). In addition, the predicted number of eggs
617 spawned at each site (WIB = 11.8 million eggs, BBY = 5.4 million eggs) is close to previous
618 estimates of fecundity for Chesapeake Bay oysters with a dry tissue weight similar to those of the
619 present study – 16.67±1.93 million eggs for WIB oysters averaging 0.70 g and 12.58±1.87
620 million eggs for BBY oysters averaging 0.62 g (Thompson et al. 1996).
621

The reduced fecundity of BBY oysters compared to WIB oysters was in part the result of the fewer predicted spawnings (one spawning for BBY versus two spawnings for WIB) over the course of the model run. The number of spawns an individual oyster undertakes under natural conditions over the course of a year in the Chesapeake Bay has not been well documented or studied empirically. However, based on temperature thresholds necessary for inducing gametogenesis, it has been predicted that oyster populations in the Chesapeake Bay can undertake up to five mass spawning events throughout the summer, and at least two of those have been empirically observed (Mann et al. 2014). Therefore, the one to two predicted spawns from the DEB model does appear to be a reasonable estimate for oysters from the area, at least at the population level. Additionally, the model predicted that low oxygen conditions would lead to asynchrony of spawning between oysters from the two sites as reduced growth in BBY oysters prevented them from reaching a sufficient GSI to spawn. Oyster spawning in the Chesapeake Bay tends to occur in pulses throughout the summer (Mann et al. 2014). For broadcast spawners, like the eastern oyster or corals, synchronicity in spawning is critical to prevent temporal reproductive isolation (Levitan et al. 2004) as well as to allow for overall success in fertilization of gametes (Levitan 1995). Thus, asynchronous spawning between oysters from reefs prone to hypoxia and oysters from reefs experiencing more normoxic conditions could lead to reduced reproductive success among hypoxia-exposed oysters.

In the model, spawning was induced by a combination of ambient temperature, accrual of degree-days above a threshold gametogenesis temperature, and a sufficient percentage of body mass allocated towards gonads (GSI). The ambient temperature necessary for inducing spawning (Shumway 1996) as well as the number of degree-days needing to be accrued have both been

studied in Chesapeake Bay oysters (Mann et al. 2014), so these parameter values are fairly well-established. However, the threshold GSI used to induce spawning is less well understood in the region. The available estimates of threshold GSI values for spawning in *C. virginica* are limited to oysters sourced from the Gulf of Mexico, Lavaud et al. (2021) with a GSI of 8 and Choi (1992) with a GSI of 20. Using either of these GSI values during model validation induced spawning at six or more timepoints throughout the model run which exceeded the predicted number of spawns oysters undergo in the bay each summer, indicating that these previously parameterized GSI values may not be suitable for Chesapeake Bay oysters. Characteristics of oyster reproduction do vary geographically (Loosanoff and Nomejko 1951) so it is possible that oysters from the more temperate climate of the Chesapeake Bay would be triggered to spawn at a higher threshold GSI. *Crassostrea gigas*, a congener of *C. virginica*, tends to inhabit more temperate habitats and their estimated threshold GSIs for spawning – ranging between 35-50 (Pouvreau et al. 2006, Thomas et al. 2016, van deer Veer 2006) – are much higher than those reported for Gulf of Mexico *C. virginica*.

Empirically measured data on oyster gonad mass was not available to validate the model predictions for reproductive output. Given that the reproductive output as measured by number of spawned eggs matched what would be expected based on oyster size (discussed above), gonad masses likely reflect accurate values of reproductive outputs. However, it is plausible that hypoxia exposure could impose additional energetic stress on oyster's reproductive activities. Hypoxia has been shown to be an endocrine disruptor in fish, limiting gametogenesis and reducing the quality of gametes (Wu et al. 2003). Without observed measurements of gonad mass for oysters from sites experiencing differing oxygen availability, it is unknown whether

668 additional constraints could be imposed on reproduction in *C. virginica*. Further parameterization
669 of the reproductive aspect of the *C. virginica* DEB model with empirical data would provide
670 more certainty in the model's reproductive outputs.
671
672 *4.4 Overall Model Caveats and Future Directions*
673 The overall fit of the model to measured oyster growth in the Chesapeake Bay indicates that the
674 model provides an accurate estimate of oyster growth even though the parameters used in this
675 DEB model were sourced from the literature and not estimated from empirical data collected on
676 geographically proximal individuals. The energetic parameters used for the study were primarily
677 parameterized for oysters sourced from the Gulf of Mexico (Lavaud et al. 2021). In general,
678 DEB parameters are well-constrained for a given species (Kooijman 2000) and, for some
679 parameters, even show similar values between closely related species (e.g., van der Veer et al.
680 2006). However, non-stationarity of DEB parameters between geographically distant populations
681 has been found, owing perhaps to local adaptation to differing environmental conditions between
682 populations (Monaco et al. 2019). For example, volume-specific somatic maintenance costs have
683 been shown to vary considerably between different parameterizations for *C. virginica*, from
684 4.166 J/cm^3/d (Lavaud and Kooijman 2018) to 38 J/cm^3/d (Lavaud et al. 2021). The difference in
685 values may indicate that this parameter is not stationary and requires additional estimation,
686 perhaps using oysters from different geographical locations to provide an optimal estimate.
687
688 The present model provides an important first step in modeling the bioenergetic effects of low
689 dissolved oxygen on adult oyster growth and reproduction, but future additions to the model will
690 allow for its application more broadly. One limitation of the present model is that it only focuses

691 on the effect of hypoxia on adult oyster growth. Hypoxia also affects bioenergetics of larval and
692 juvenile oysters, as indicated by reduced feeding rates, reduced growth rates, increased mortality,
693 and delayed development (Baker and Mann 1992, Baker and Mann 1994, Widdows et al. 1989).
694 However, the current parameterization of the oxygen correction factor may not be easily
695 transferable to earlier oyster life-stages because metabolic responses to hypoxia do appear to
696 vary ontogenetically in other marine invertebrates (Leiva et al. 2018). A key advantage of DEB
697 models is in the ability to follow an individual throughout their full life cycle, so incorporating
698 larvae and juveniles into the model is crucial. Future work integrating additional life-stages into
699 the model will allow for better predictions of how hypoxia exposure will affect oysters over their
700 complete life cycle but requires targeted experimentation at each life stage.
701
702 Additionally, the model assumes additive effects of salinity and temperature on oyster
703 bioenergetics, which may not accurately reflect oyster response to co-occurring temperature or
704 salinity stress. The environmental data used to force the current model did not expose the oysters
705 to any extremes in either temperature or salinity so interactions between stressors did not
706 complicate the present study. However, there is potential for synergism between temperature and
707 salinity stress and low oxygen stress on organismal energetics (e.g., Wang et al. 2011, Marcek et
708 al. 2020) and these should be considered in future model iterations. In the Chesapeake Bay,
709 increases in the incidence of both high temperatures and hyposalinity are expected with climate
710 change, which would likely coincide with periods of seasonal hypoxia (Najjar et al. 2010).
711 However, there is currently limited empirical data available on the energetic effects of co-
712 occurring stressors with hypoxia for *C. virginica*. Future studies that examine the interactions
713 between stressors on *C. virginica* energetics would be valuable for use with the model, allowing

for more accurate predictions of long-term effects of hypoxia and co-occurring stressors on oysters.

5. Conclusions

Integration of dissolved oxygen into the DEB model for *C. virginica* provides an important first step in the ability to mechanistically predict the effects of hypoxic exposure on oyster growth and reproduction. The model developed in the present study indicates that exposure to hypoxia decreases oyster shell and tissue growth and leads to decreases in oyster fecundity, as well as changes to spawning frequency. Future empirical studies focusing on the potential for cumulative effects of temperature, salinity, and dissolved oxygen stress on oyster energetics, as well as influences of hypoxia on oyster reproduction would allow for more confidence in model outputs. Additionally, incorporation of early life-stages into the model will allow for predictions to be made across the full life cycle of *C. virginica*. While this additional work will increase the versatility of the model, in its current iteration, the ability of the model to accurately predict adult oyster growth under differing oxygen regimes makes it an important tool to make predictions about how oysters will respond to the increased frequency of hypoxic exposures that are expected in the future due to climate change.

Acknowledgements

The authors would like to thank Darryl Hondorp and Denise Breitburg for supplying data that contributed substantially to the development of this model. This manuscript was greatly improved by feedback from Alexandra Bely, James Pierson, Christopher Rowe, Romain Lavaud,

and two anonymous reviewers. This work was supported by funding from the Marine, Estuarine, and Environmental Science Graduate Program at the University of Maryland.

Literature Cited

Aguirre-Velarde, A., Pecquerie, L., Jean, F., Thouzeau, G., Flye-Sainte-Marie, J. 2019a. Predicting the energy budget of the scallop *Argopecten purpuratus* in an oxygen-limiting environment. *Journal of Sea Research*. 143:254-261. https://doi.org/10.1016/j.seares.2018.09.011

Aguirre-Velarde, A., Thouzeau, G., Jean, F., Mendo, J., Cueto-Vega, R., Kawazo-Delgado, M., Vásquez-Spencer, J., Herrera-Sanchez, D., Vega-Espinoza, A., Flye-Sainte-Marie, J. 2019b. Chronic and severe hypoxic conditions in Paracas Bay, Pisco, Peru: Consequences on scallop growth, reproduction, and survival. *Aquaculture*. 512:734259. https://doi.org/10.1016/j.aquaculture.2019.734259

Baker, S.M., Mann, R. 1992. Effects of hypoxia and anoxia on larval settlement, juvenile growth, and juvenile survival of the oyster *Crassostrea virginica*. *The Biological Bulletin*. 182(2):265-269. https://doi.org/10.2307/1542120

Baker, S.M., and R. Mann. 1994. Description of metamorphic phases in the oyster *Crassostrea virginica* and effects of hypoxia on metamorphosis. *Marine Ecology Progress Series*. 104:91-99. https://www.jstor.org/stable/24842601

Barber, B.J., Ford, S.E., and R.N. Wargo. 1991. Genetic variation in the timing of gonadal maturation and spawning of the eastern oyster, *Crassostrea virginica* (Gmelin). *Biological Bulletin*. 181:216-221. https://doi.org/10.2307/1542092

Bernard, I., de Kermoysan, G., and S. Pouvreau. 2011. Effect of phytoplankton and temperature on the reproduction of the Pacific oyster *Crassostrea gigas*: Investigation through DEB

759 theory. *Journal of Sea Research*. 66(4):349–360.
760 https://doi.org/10.1016/j.seares.2011.07.009

761 Breitburg, D. 1990. Near-shore hypoxia in the Chesapeake Bay: Patterns and relationships
762 among physical factors. *Estuarine, Coastal and Shelf Science*. 30(6):592-609.
763 https://doi.org/10.1016/0272-7714(90)90095-9

764 Breitburg, D., Levin, L.A., Oschlies, A., Grégoire, M., Chavez, F.P., Conley, D.J., Garçon, V.,
765 Gilbert, D., Gutiérrez, D., Isensee, K., Jacinto, G.S., Limburg, K.E., Montes, I., Naqvi,
766 S.W.A., Pitcher, G.C., Rabalais, N.N., Roman, M.R., Rose, K.A., Seibel, B.A., Telszewski,
767 M., Yasuhara, M., Zhang, J., 2018. Declining oxygen in the global ocean and coastal
768 waters. Science. 359, eaam7240. https://doi.org/10.1126/science.aam7240

769 Breitburg, D.L., Hondorp, D., Audemard, C., Carnegie, R.B., Burrell, R.B., Trice, M., and V.
770 Clark. 2015. Landscape-level variation in disease susceptibility related to shallow-water
771 hypoxia. *PLoS ONE*. 10(2):e0116223. https://doi.org/10.1371/journal.pone.0116223

772 Casas, S.M., Lavaud, R., La Peyre, M.K., Comeau, L.A., Filgueira, R., and J.F. La Peyre. 2018.
773 Quantifying salinity and season effects on eastern oyster clearance and oxygen
774 consumption rates. *Marine Biology*. 165(5):1-13. https://doi.org/10.1007/s00227-018-
775 3351-x

776 Choi, K. 1992. *A study on the reproduction of oysters, Crassostrea virginica (Pelecypoda;*
777 *Mollusca) in the Galveston Bay area, Texas, using immunological techniques.* Texas
778 A&M University, Galveston, Texas.

779 Clark, V. 2014. The effects of diel-cycling hypoxia and hypercapnia on eastern oyster,
780 *Crassostrea virginica* (Gmelin), clearance rates and hemolymph pH. *College Park, MD:*
781 *University of Maryland Center for Environmental Science.*

782 Coakley, J.M. 2004. Growth of eastern oyster, *Crassostrea virginica*, in Chesapeake Bay.
783 *College Park, MD: University of Maryland College Park.*

784 Coen, L.D., Brumbaugh, R.D., Bushek, D., Grizzle, R., Luckenbach, M.W., Posey, M.H.,
785 Powers, S.P., and S.G. Tolley. 2007. Ecosystem services related to oyster restoration.
786 *Marine Ecology Progress Series*. 341:303-307. https://doi.org/10./3354/meps341303

787 Dame, R.F. 1979. The abundance, diversity, and biomass of macrobenthos on North Inlet, South
788 Carolina, intertidal oyster reefs. *Proceedings of the National Shellfisheries Association*.
789 69:6-10.

790 Diaz, R.J., and R. Rosenberg. 1995. Marine benthic hypoxia: A review of its ecological effects
791 and the behavioural responses of benthic macrofauna. *Oceanography and Marine*
792 *Biology - An Annual Review*. 33:245–303.

793 Eby, L.A., Crowder, L.B., McClellan, C.M., Peterson, C.H., and M.J. Powers. 2005. Habitat
794 degradation from intermittent hypoxia: impacts on demersal fishes. *Marine Ecology*
795 *Progress Series*. 291:249-261. https://doi.org/10.3354/meps291249

796 Eggleston, D.B. 1990. Foraging behavior of the blue crab, *Callinectes sapidus*, on juvenile
797 oysters, *Crassostrea virginica*: Effects of prey density and size. *Bulletin of Marine*
798 *Science*. 46(1):62-82.

Filgueira, R., Guyondet, T., Comeau, L.A., and J. Grant. 2014. A fully-spatial ecosystem-DEB model of oyster (*Crassostrea virginica*) carrying capacity in the Richibucto Estuary, Eastern Canada. *Journal of Marine Systems*. 136:42-54. https://doi.org/10.1016/j.jmarsys.2014.03.015

Galic, N., Grimm, V., and V.E. Forbes. 2017. Impaired ecosystem process despite little effects on populations: modeling combined effects of warming and toxicants. *Global Change Biology*. 23(8): 2973-2989. https://doi.org/10.1111/gcb.13581

Galtsoff, P.S. 1964. The American Oyster *Crassostrea virginica* Gmelin. *Fisheries Bulletin of the Fish and Wildlife Service*. 64:1-480. https://doi.org/10.2307/1350854

Gobler, C.J., Clark, H.R., Griffith, A.W., and M.W. Lusty. 2017. Diurnal fluctuations in acidification and hypoxia reduce growth and survival of larval and juveniles bay scallops (*Argopecten irradians*) and hard clams (*Mercenaria mercenaria*). *Frontiers in Marine Science*. 3:282. https://doi.org/10.3389/fmars.2016.00282

Gobler, C.J., DePasquale, E.L., Griffith, A.W., and H. Baumann. 2014. Hypoxia and acidification have additive and synergistic negative effects on the growth, survival, and metamorphosis of early stage bivalves. *PloS One*. 9(1):e83648. https://doi.org/10.1371/journal.pone.0083648.

Grabowski, J.H., and C.H. Peterson. 2007. Restoring oyster reefs to recover ecosystem services. In: *Ecosystem engineers: Plants to Protists*. Eds. Cuddington, K., Hastings, A., Byers, J.E., and Wilson, W. Pp.281-298.

819 Herreid, C.F. 1980. Hypoxia in invertebrates. *Comparative Biochemistry and Physiology A*.
820 67:311-320. https://doi.org/10.1016/S0300-9629(80)80002-8

821 Hicks, D.W., and R.F. McMahon. 2002. Respiratory responses to temperature and hypoxia in the
822 nonindigenous brown mussel, *Perna perna* (Bivalvia: Mytilidae), from the Gulf of
823 Mexico. *Journal of Experimental Marine Biology and Ecology*. 277:61-78.
824 https://doi.org/10.1016/S0022-0981(02)00276-9

825 Hicks, D.W., and R.F. McMahon. 2005. Effects of temperature on chronic hypoxia tolerance in
826 the non-indigenous brown mussel *Perna perna* (Bivalvia: Mytilidae) from the Texas Gulf
827 of Mexico. *Journal of Molluscan Studies*. 71(4):410-408.
828 https://doi.org/10.1093/mollus/eyi042

829 Jackson, J.B.C., Kirby, M.X., Berger, W.M., Bjorndal, K.A., Botsford, L.W., Bourque, B.J.,
830 Bradbury, R.H., Cooke, R., Erlandson, J., Estes, J.A., Hughes, T.P., Kidwell, S., Lange,
831 C.B., Lenihan, H.S., Pandolfi, J.M., Peterson, C.H., Steneck, R.S., Tegner, M.J., and R.R.
832 Warner. 2001. Historical overfishing and the recent collapse of coastal ecosystems.
833 *Science*. 293:629-638. https://doi.org/10.1126/science.1059199

834 Johnson, M.W., Powers, S.P., Senne, J., and K. Park. 2009. Assessing in situ tolerances of
835 Eastern oysters (*Crassostrea virginica*) under moderate hypoxic regimes: Implications
836 for restoration. *Journal of Shellfish Research.* 28(2):185-192.
837 https://doi.org/10.2983/035.028.0202

838 Kennedy, V.S., and L.B. Krantz. 1982. Comparative gametogenic and spawning patterns of the
839 oyster *Crassostrea virginica* (Gmelin) in central Chesapeake Bay. *Journal of Shellfish*
840 *Research*. 2(2):133-140.

841 Keppel, A.G., Breitburg, D.L., Wikfors, G.H., Burrell, R.B., and V.M. Clark. 2015. Effects of
842 co-varying diel-cycling hypoxia and pH on disease susceptibility in the eastern oyster
843 *Crassostrea virginica*. *Marine Ecology Progress Series*. 538:169-183.
844 https://doi.org/10.3354/meps11479

845 Kirby, M.X. 2004. Fishing down the coast: Historical expansion and collapse of oyster fisheries
846 along continental margins. *Proceedings of the National Academy of Sciences*. 101:13096-
847 13099. https://doi.org/10.1073/pnas.0405150101
848 Kooijman, S.A.L.M. 1986. Energy budgets can explain body size relations. *Journal of*
849 *Theoretical Biology*. 121:269-282. https://doi.org/10.1016/S0022-5193(86)80107-2

850 Kooijman, S.A.L.M. 2000. Dynamic Energy and Mass Budgets in Biological Systems.
851 Cambridge University Press, Cambridge, UK, 424 pp.

852 Kooijman, S.A.L.M. 2010. Dynamic Energy Budget Theory for Metabolic Organisation.
853 Cambridge University Press, Cambridge, UK, 514 pp.

854 Lavaud, R., Flye-Sainte-Marie, J., Jean, F., Emmery, A., Strand, A., and S.A.L.M. Kooijman.
855 2014. Feeding and energetics of the great scallop, *Pecten maximus*, through a DEB
856 model. *Journal of Sea Research*. 94:5-18. https://doi.org/10.1016/j.seares.2013.10.011

Lavaud, R., La Peyre, M.K., Casas, S.M., Bacher, C., and J.F. La Peyre. 2017. Integrating the effects of salinity on the physiology of the eastern oyster, *Crassostrea virginica*, in the northern Gulf of Mexico through a Dynamic Energy Budget model. *Ecological Modeling*. 363:221-233. https://doi.org/10.1016/j.ecolmodel.2017.09.003

Lavaud, R., and B. Kooijman. 2018. AmP *Crassostrea virginica*. Version 2018/08/27 https://www.bio.vu.nl/thb/deb/deblab/add_my_pet/entries_web/Crassostrea_virginica/Crassostrea_virginica_res.html

Lavaud, R., Thomas, Y., Pecquerie, L., Benoît, H., Guyondet, T., Flye-Sainte-Marie, J., and D. Chabot. 2019. Modeling the impact of hypoxia on the energy budget of Atlantic cod in two populations of the Gulf of Saint-Lawrence, Canada. *Journal of Sea Research*. 143:243-253. https://doi.org/10.1016/j.seares.2018.07.001

Lavaud, R., La Peyre, M.K., Justic, D., and J.F. La Peyre. 2021. Dynamic Energy Budget modelling to predict eastern oyster growth, reproduction, and mortality under river management and climate change scenarios. *Estuarine, Coastal and Shelf Science*. 251:1–22. https://doi.org/10.1016/j.ecss.2021.107188

Lavaud, R., La Peyre, M.K., Couvillion, B., Pollack, J.B., Brown, V., Palmer, T.A. and Keim, B. 2024. Predicting restoration and aquaculture potential of eastern oysters through an eco-physiological mechanistic model. *Ecological Modelling*. 489, p.110603.

Laurent, A., Fennel, K., Ko, D.S., and J. Lehrter. 2018. Climate change projected to exacerbate impacts of coastal eutrophication in the northern Gulf of Mexico. *Journal of Geophysical Research: Oceans*. 123:3408-3426. https://doi.org/10.1002/2017JC013583

878 Leiva, F.P., Garcés, C., Verberk, W.C.E.P., Care, M., Paschke, K., and P. Gebauer. 2018.
879 Differences in the respiratory response to temperature and hypoxia across four life-stages
880 of the intertidal porcelain crab *Petrolisthes laevigatus*. *Marine Biology*. 165:146.
881 https://doi.org/10.1007/s00227-018-3406-z

882 Levitan, D.R. 1995. "The ecology of fertilization in free-spawning invertebrates." In *Ecology of*
883 *Marine Invertebrate Larvae*. Ed. McEdward, L.R. CRC Press, Boca Raton, FL. P. 124-
884 152.

885 Levitan, D.R., Fukami, H., Jara, J., Kline, D., McGovern, T.M., McGhee, K.E., Swanson, C.A.,
886 and N. Knowlton. 2004. Mechanisms of reproductive isolation among sympatric
887 broadcast-spawning corals of the *Montastraea annularis* species
888 complex. *Evolution*. 58(2):308-323. https://doi.org/10.1111/j.0014-3820.2004.tb01647.x

889 Long, W.C., Seitz, R.D., Brylawski, B., and R.N. Lipcius. 2014. Individual, population, and
890 ecosystem effects of hypoxia on a dominant benthic bivalve in Chesapeake Bay.
891 *Ecological Monographs*. 82(2):303–327. https://doi.org/10.1890/13-0440.1

892 Loosanoff, V.L., and C.A. Nomejko. 1951. Existence of physiologically-different races of
893 oysters, *Crassostrea virginica*. *The Biological Bulletin*. 101(2):51-156.
894 https://www.jstor.org/stable/1538381

895 Mann, R., Southworth, M., Carnegie, R.B., and R.K. Crockett. 2014. Temporal variation in
896 fecundity and spawning in the eastern oyster, *Crassostrea virginica*, in the Piankatank
897 River, Virginia. *Journal of Shellfish Research*. 33(1):167-176.
898 https://doi.org/10.2983/035.033.0116

899 Marcek, B.J., Burbacher, E.A., Dabrowski, K., Winslow, K.P., and S.A. Ludsin. 2020.
900 Interactive effects of hypoxia and temperature on consumption, growth, and condition of
901 juvenile hybrid striped bass. *Transactions of the American Fisheries Society.* 149(1):71-
902 83. https://doi.org/10.1002/tafs.10210

903 Marcus, N.H., Richmond, C., Sedlacek, C., Miller, G.A., and C. Oppert. 2004. Impact of hypoxia
904 on the survival, egg production and population dynamics of *Acartia tonsa* Dana. *Journal*
905 *of Experimental Marine Biology and Ecology*. 301:111-128.
906 https://doi.org/10.1016/j.jembe.2003.09.016

907 McFarland, K.M. 2015. *Population dynamics of the invasive green mussel Perna viridis and*
908 *their response to the toxic dinoflagellate Karenia brevis: Application of Dynamic Energy*
909 *Budget theory to determine population trends.* Université de Bretagne Occidentale, Brest,
910 France.

911 Monaco, C.J., Porporato, E.M., Lathlean, J.A., Tagliarolo, M., Sarà, G., and C.D. McQuaid.
912 2019. Predicting the performance of cosmopolitan species: Dynamic energy budget
913 model skill drops across large spatial scales. *Marine Biology*. 166(2):14.
914 https://doi.org/10.1007/s00227-018-3462-4

915 Najjar, R.G., Pyke, C.R., Adams, M.B., Breitburg, D., Hershner, C., Kemp, M., Howarth, R.,
916 Mulholland, M.R., Paolisso, M., Secor, D., Sellner, K., Wardrop, D., and R. Wood. 2010.
917 Potential climate-change impacts on the Chesapeake Bay. *Estuarine, Coastal and Shelf*
918 *Science*. 86(1):1–20. https://doi.org/10.1016/j.ecss.2009.09.026

Nestlerode, J.A., and R.J. Diaz. 1998. Effects of periodic environmental hypoxia on predation of a tethered polychaete, *Glycera americana*: Implications for trophic dynamics. *Marine Ecology Progress Series*. 172:185-195. https://doi.org/10.3354/meps172185

Ni, W., Li, M., Ross, A.C., and R.G. Najjar. 2019. Large projected decline in dissolved oxygen in a eutrophic estuary due to climate change. *Journal of Geophysical Research: Oceans*. 124:8271-8289. https://doi.org/10.1029/2019JC015274

Paynter, K.T., and E.M. Burreson. 1991. Effects of *Perkinsus marinus* infection in the eastern oyster, *Crassostrea virginica*: II. Disease development and impact on growth rate at different salinities. *Journal of Shellfish Research*. 10(2):425-431.

Paynter, K.T., and L. DiMichele. 1990. Growth of tray-cultured oysters (*Crassostrea virginica* Gmelin) in Chesapeake Bay. *Aquaculture*. 87:289-297. https://scholarworks.wm.edu/vimsarticles/1278

Pollack, J.B., Kim, H.C., Morgan, E.K., and P.A. Montagna. 2011. Role of flood disturbance in natural oyster (*Crassostrea virginica*) population maintenance in an estuary in South Texas, USA. *Estuaries and Coasts*. 34(1):187-197. https://doi.org/10.1007/s12237-010-9338-6

Pouvreau, S., Bourles, Y., Lefebvre, S., Gangnery, A., and M. Alunno-Bruscia. 2006. Application of a dynamic energy budget model to the Pacific oyster, *Crassostrea gigas*, reared under various environmental conditions. *Journal of Sea Research*. 56(2):156-167. https://doi.org/10.1016/j.seares.2006.03.007

939 Price, K.S., Jr., and D.L. Mauer. 1971. Holding and spawning Delaware Bay oyster (*Crassostrea*
940 *virginica*) out of season. II. Temperature requirements for maturation of gonads.
941 *Proceedings of the National Shellfisheries Association*. 61:29-34.

942 Rabalais, N.N., Díaz, R.J., Levin, L.A., Turner, R.E., Gilbert, D., and J. Zhang. 2010. Dynamics
943 and distribution of natural and human-caused hypoxia. *Biogeosciences*. 7(2):585–619.
944 https://doi.org/10.5194/bg-7-585-2010

945 Rogers, N.J., Urbina, M.A., Reardon, E.E., McKenzie, D.J., and R.W. Wilson. 2016. A new
946 analysis of hypoxia tolerance in fishes using a database of critical oxygen level (P_{crit}).
947 *Conservation Physiology*. 4(1):cow012. https://doi.org/10.1093/conphys/cow012

948 Rosland, R., Strand, Ø., Alunno-Bruscia, M., Bacher, C., and T. Strohmeier. 2009. Applying
949 Dynamic Energy Budget (DEB) theory to simulate growth and bio-energetics of blue
950 mussels under low seston conditions. *Journal of Sea Research*. 62:49-61.
951 https://doi.org/10.1016/j.seares.2009.02.007

952 Shumway, S.E. 1996. "Natural Environmental Factors" In *The Eastern Oyster Crassostrea*
953 *virginica*, (eds.) V.S. Kennedy, C.R. Newell, and A.F. Eble College Park, MD: Maryland
954 Sea Grant College, pp. 467-513.

955 Shumway, S.E., Koehn, R.K., 1982. Oxygen consumption in the American oyster *Crassostrea*
956 *virginica*. Mar. Ecol. Prog. Ser. 9, 59-68. https://jstor.org/stable/24814571

957 Smyth, A.R., Geraldi, N.R., and M.F. Piehler. 2013. Oyster-mediated benthic-pelagic coupling
958 modifies nitrogen pools and processes. *Marine Ecology Progress Series*. 493:23-30.
959 https://doi.org/10.3354/meps10516

960 Sobral, P., and J. Widdows. 1997. Influence of hypoxia and anoxia on the physiological
961 responses of the clam *Ruditapes decassatus* from southern Portugal. *Marine Biology*.
962 127:455-461. https://doi.org/10.1007/s002270050033

963 Sollid, J., De Angelis, P., Gundersen, K., and G.E. Nilsson. 2003. Hypoxia induces adaptive and
964 reversible gross morphological changes in crucian carp gills. *Journal of Experimental*
965 *Biology*. 206(20):3667-3673. https://doi.org/10.1242/jeb.00594

966 Soniat, T.M., Cozelmann, C.P., Byrd, J.D., Roszell, D.P., Bridevaux, J.L., Suir, K.J., and S.B.
967 Colley. 2013. Predicting the effects of proposed Mississippi River diversions on oyster
968 habitat quality: application of an oyster habitat suitability index model. *Journal of*
969 *Shellfish Research*. 32(3):381-394. https://doi.org/10.2983/035.032.0302

970 Stevens, A.M., and C.J. Gobler. 2018. Interactive effects of acidification, hypoxia, and thermal
971 stress on growth, respiration, and survival of four North Atlantic bivalves. *Marine*
972 *Ecology Progress Series*. 604:143-161. https://doi.org/10.3354/meps12725

973 Stickle, W.B., Kapper, M.A., Liu, L-L., Gnaiger, E., and S.Y. Wang. 1989. Metabolic
974 adaptations of several species of crustaceans and molluscs to hypoxia: Tolerance and
975 microcalorimetric studies. *Biological Bulletin.* 177: 303-312.
976 https://doi.org/10.2307/1541945

977 Taylor, A.C., and A.R. Brand. 1975. Effects of hypoxia and body size on the oxygen
978 consumption of the bivalve *Arctica islandica* (L.). *Journal of Experimental Marine*
979 *Biology and Ecology*. 19:187-196. https://doi.org/10.1016/0022-0981(75)90046-5

980 Thomas, Y., Pouvreau, S., Alunno-Bruscia, M., Barillé, L., Gohin, F., Bryère, P., and P. Gernez.
981 2016. Global change and climate-driven invasion of the Pacific oyster (*Crassostrea*
982 *gigas*) along European coasts: A bioenergetics modelling approach. *Journal of*
983 *Biogeography.* 43:568-579. https://doi.org/10.1111/jbi.12665

984 Thomas, Y., Flye-Sainte-Marie, J., Chabot, D., Aguirre-Velarde, A., Marques, G.M., and L.
985 Pecquerie. 2019. Effects of hypoxia on metabolic functions in marine organisms:
986 Observed patterns and modelling assumptions within the context of Dynamic Energy
987 Budget (DEB) theory. *Journal of Sea Research*. 143:231–242.
988 https://doi.org/10.1016/j.seares.2018.05.001

989 Thompson, R.J., Newell, R.I.E, Kennedy, V.S., and R. Mann. 1996. "Reproductive Processes
990 and Early Development" In *The Eastern Oyster Crassostrea virginica*, eds V.S. Kennedy,
991 C.R. Newell, and A.F. Eble, College Park, MD: Maryland Sea Grant College, pp.335-
992 370.

993 Van der Veer, H.W., Cardoso, J.F.M.F., and J. van der Meer. 2006. The estimation of DEB
994 parameters for various Northeast Atlantic bivalve species. *Journal of Sea Research*.
995 *56*(2):107–124. https://doi.org/10.1016/j.seares.2006.03.005

Vaquer-Sunyer, R., and C.M. Duarte. 2008. Thresholds of hypoxia for marine biodiversity. *Proceedings of the National Academy of Science*. 105(40):15452-15457. https://doi.org/10.1073/pnas.0803833105

Wang, W.X., and J. Widdows. 1993. Metabolic responses of the common mussel *Mytilus edulis* to hypoxia and anoxia. *Marine Ecology Progress Series*. 95:205-214. https://www.jstor.org/stable/24832887

Wang, Y., Hu, M., Wong, W. H., Shin, P. K., and S.G. Cheung. 2011. The combined effects of oxygen availability and salinity on physiological responses and scope for growth in the green-lipped mussel *Perna viridis*. *Marine Pollution Bulletin*. 63(5-12):255-261. https://doi.org/10.1016/j.marpolbul.2011.02.004

Watson, S.-A., Morley, S.A., and L.S. Peck. 2017. Latitudinal trends in shell production cost from the tropics to the poles. *Science Advances*. 3:e1701362. https://doi.org/10.1126/sciadv.1701362

Widdows, J., Newell, R.I.E., and R. Mann. 1989. Effects of hypoxia and anoxia on survival, energy metabolism, and feeding of oyster larvae (*Crassostrea virginica*, Gmelin). *The Biological Bulletin*. 177(1):154-166. https://doi.org/10.2307/1541843

Wu, R.S.S., Zhou, B.S., Randall, D.J., Woo, N.Y.S., and P.K.S. Lam. 2003. Aquatic hypoxia is an endocrine disruptor and impairs fish reproduction. *Environmental Science and Technology*. 37:1137-1141. https://doi.org/10.1021/es0258327

1015 Zu Ermgassen, P.S., Spalding, M.D., Grizzle, R.E., and R.D. Brumbaugh. 2013. Quantifying the
1016 loss of a marine ecosystem service: filtration by the eastern oyster in US
1017 estuaries. *Estuaries and Coasts*. 36(1):36-43. https://doi.org/10.1007/s12237-012-9559-y

Supplementary Table 1: Sample sizes of oysters measured for length that were used in the validation of the DEB model. Sites with oysters deployed in 2008 (CBL, CCR, BWH, SMC, and YEO) had one midpoint measurement, whereas sites with oysters deployed in 2009 (HCR, LMN, and MUL) had three midpoint measurements.

Site	Initial	Midpoint 1	Midpoint 2	Midpoint 3	Final
CBL	120	18	-	-	91
CCR	120	18	-	-	91
BWH	120	18	-	-	95
HCR	161	41	24	42	97
LMN	160	41	24	43	124
MUL	160	45	25	43	126
SMC	120	18	-	-	81
YEO	120	18	-	-	92

Supplementary Table 2: Percentage of datapoints requiring interpolation for each of the environmental datasets used in model development and predictions.

Site	Use	Temperature (°C)	Chlorophyll-*a* (*μ*g/l)	Salinity (ppt)	Dissolved Oxygen (mg/l)
CBL	Validation	0%	0%	0%	0%
CCR	Validation	13.2%	13.3%	13.3%	13.3%
BWH	Validation	4.3%	4.5%	4.3%	4.3%
HCR	Validation	5.0%	11.2%	1.8%	4.8%
LMN	Validation	7.5%	24.2%	7.5%	7.5%
MUL	Validation	14.1%	15.3%	0.02%	<0.01%
SMC	Validation	0%	0.72%	0%	0%
YEO	Validation	8.9%	8.9%	8.9%	8.9%
BBY	Prediction	6.1%	7.2%	6.1%	11.9%
WIB	Prediction	6.9%	13.9%	10.3%	29.9%

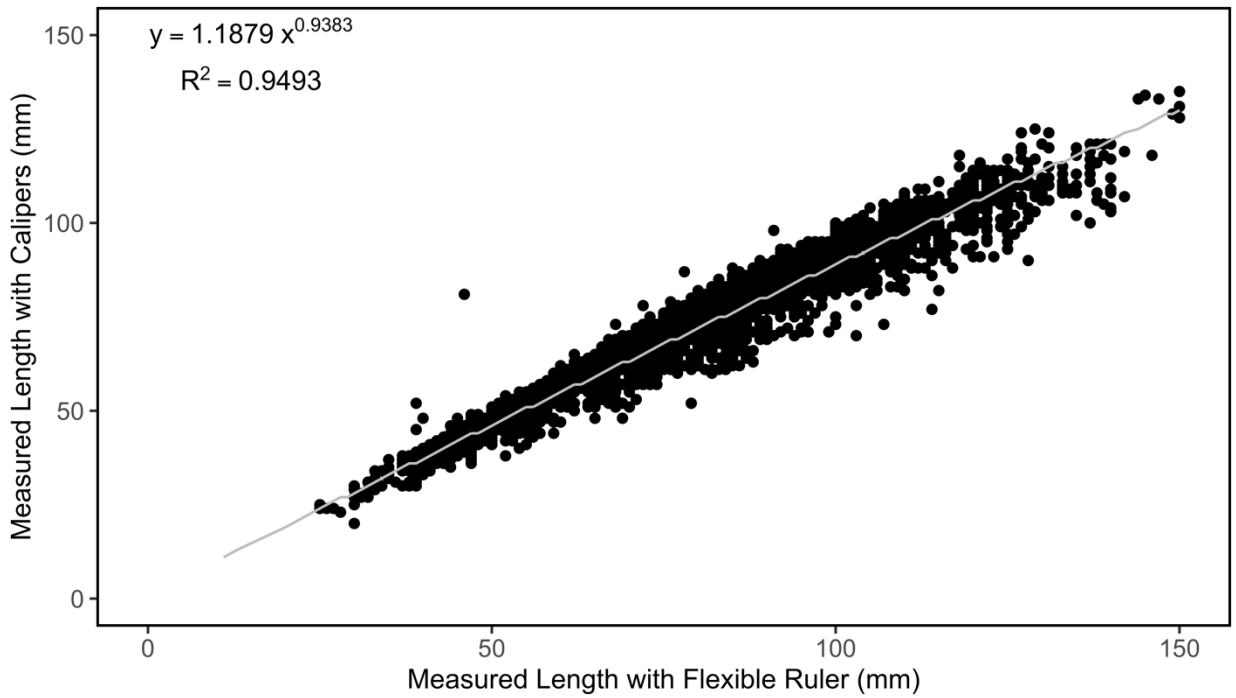

Supplementary Figure 1: Comparison of shell lengths measured with a flexible ruler versus calipers for the validation growth data. Grey line denotes best fit power function ($p<0.001$).

1034

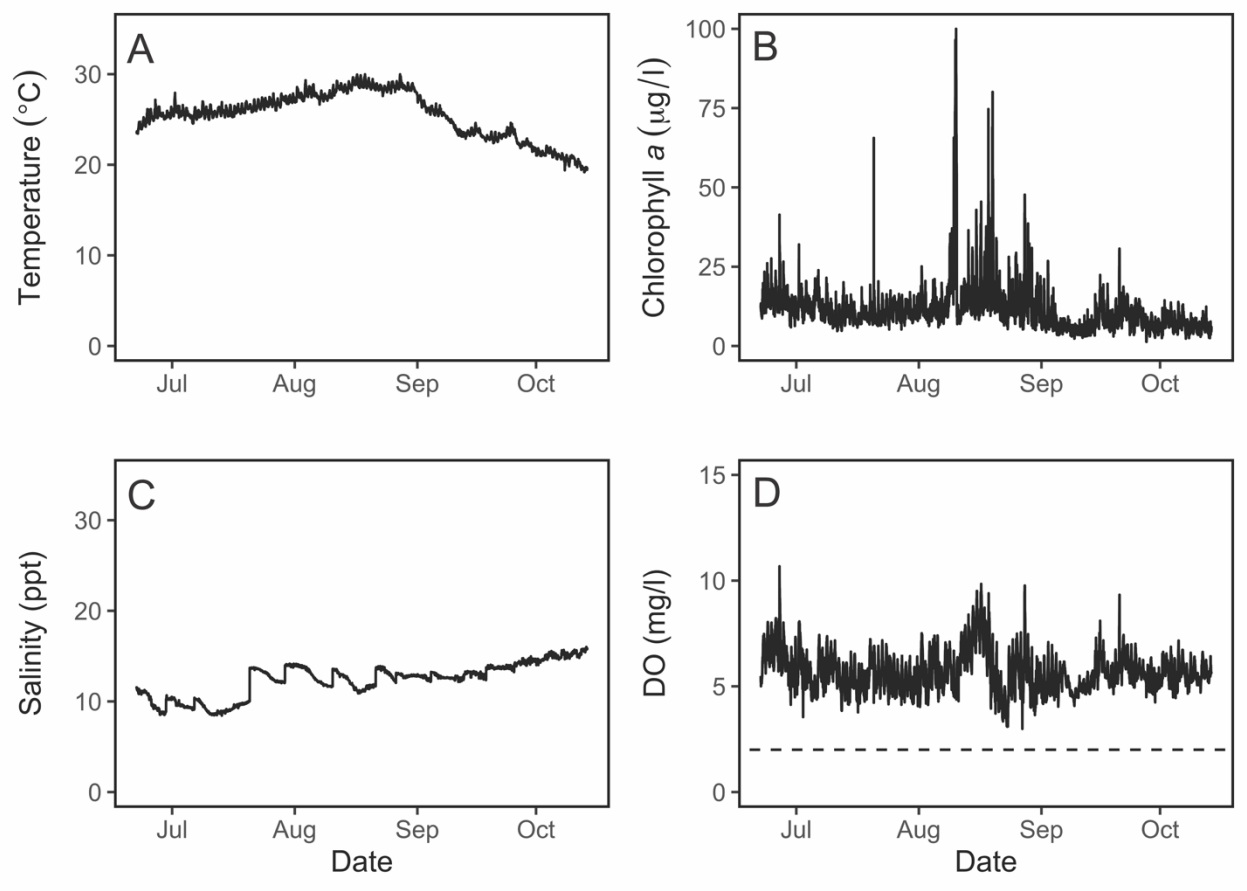

1035

1036 Supplementary Figure 2: Environmental data for the validation oyster growth dataset at
1037 Chesapeake Biological Lab (CBL). A) Temperature (°C), B) Chlorophyll *a* (μg/l), C) Salinity
1038 (ppt) and D) Dissolved oxygen (mg/l). The dashed line on the dissolved oxygen panel
1039 correspond to 2.0 mg/l or hypoxic conditions.

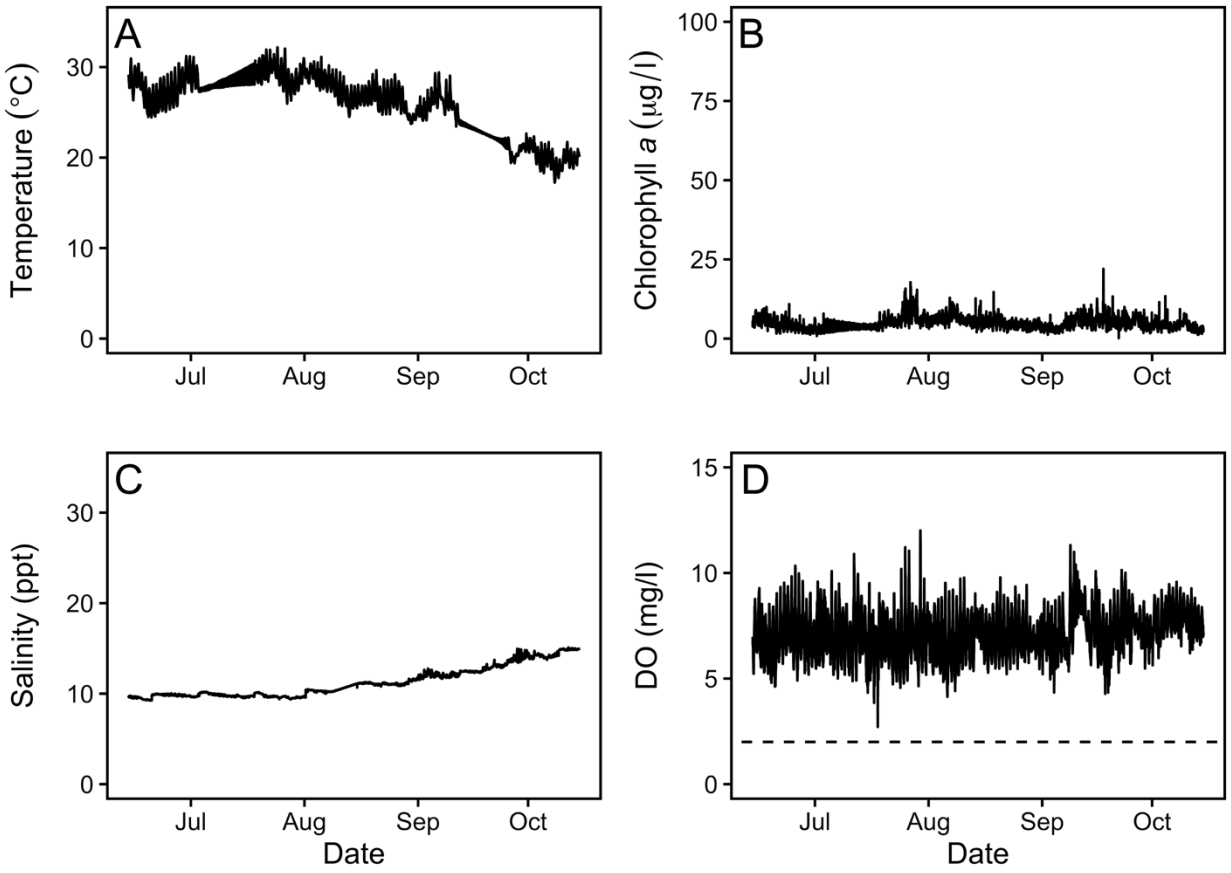

Supplementary Figure 3: Environmental data for the validation oyster growth dataset at Mulberry Point (MUL). A) Temperature (°C), B) Chlorophyll *a* (μg/l), C) Salinity (ppt) and D) Dissolved oxygen (mg/l). The dashed line on the dissolved oxygen panel correspond to 2.0 mg/l or hypoxic conditions.

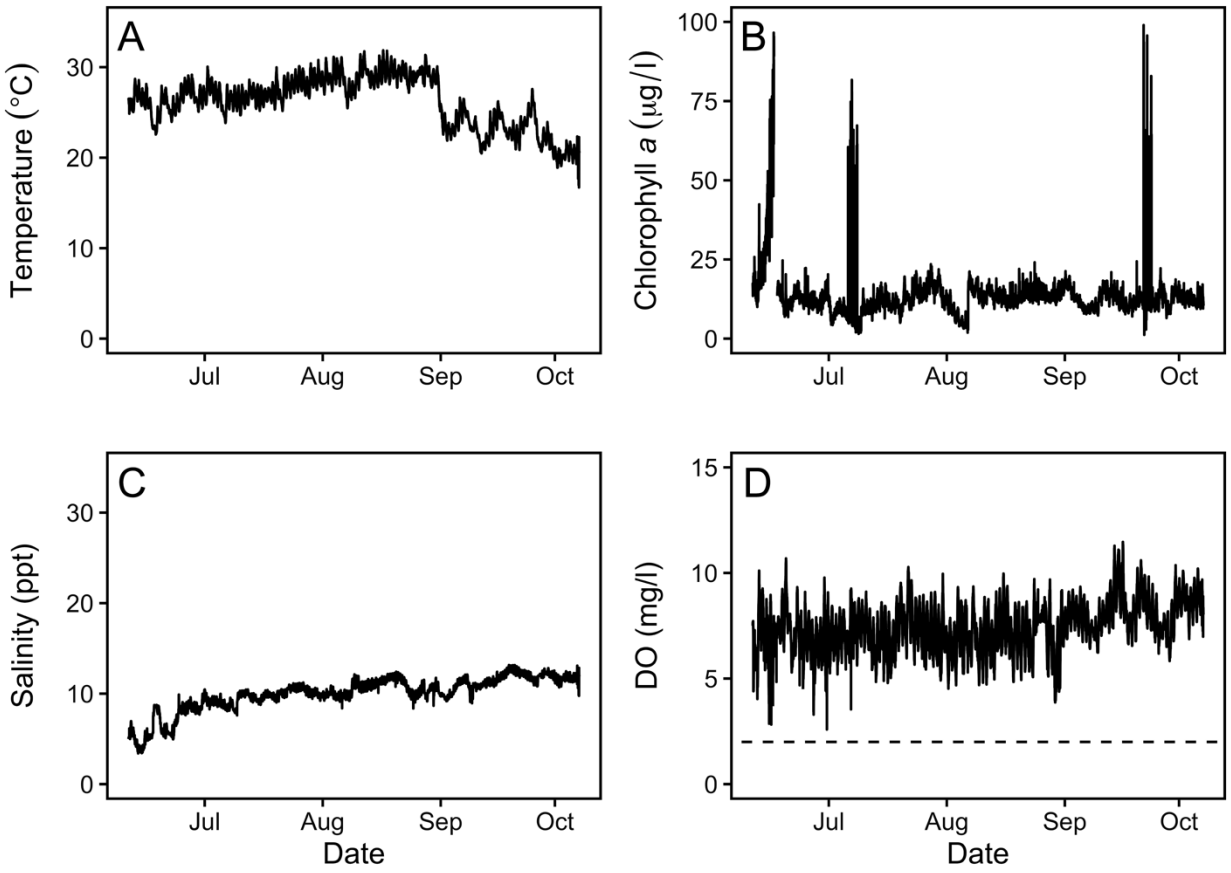

Supplementary Figure 4: Environmental data for the validation oyster growth dataset at Bowler's Wharf (BWH). A) Temperature (°C), B) Chlorophyll *a* (μg/l), C) Salinity (ppt) and D) Dissolved oxygen (mg/l). The dashed line on the dissolved oxygen panel correspond to 2.0 mg/l or hypoxic conditions.

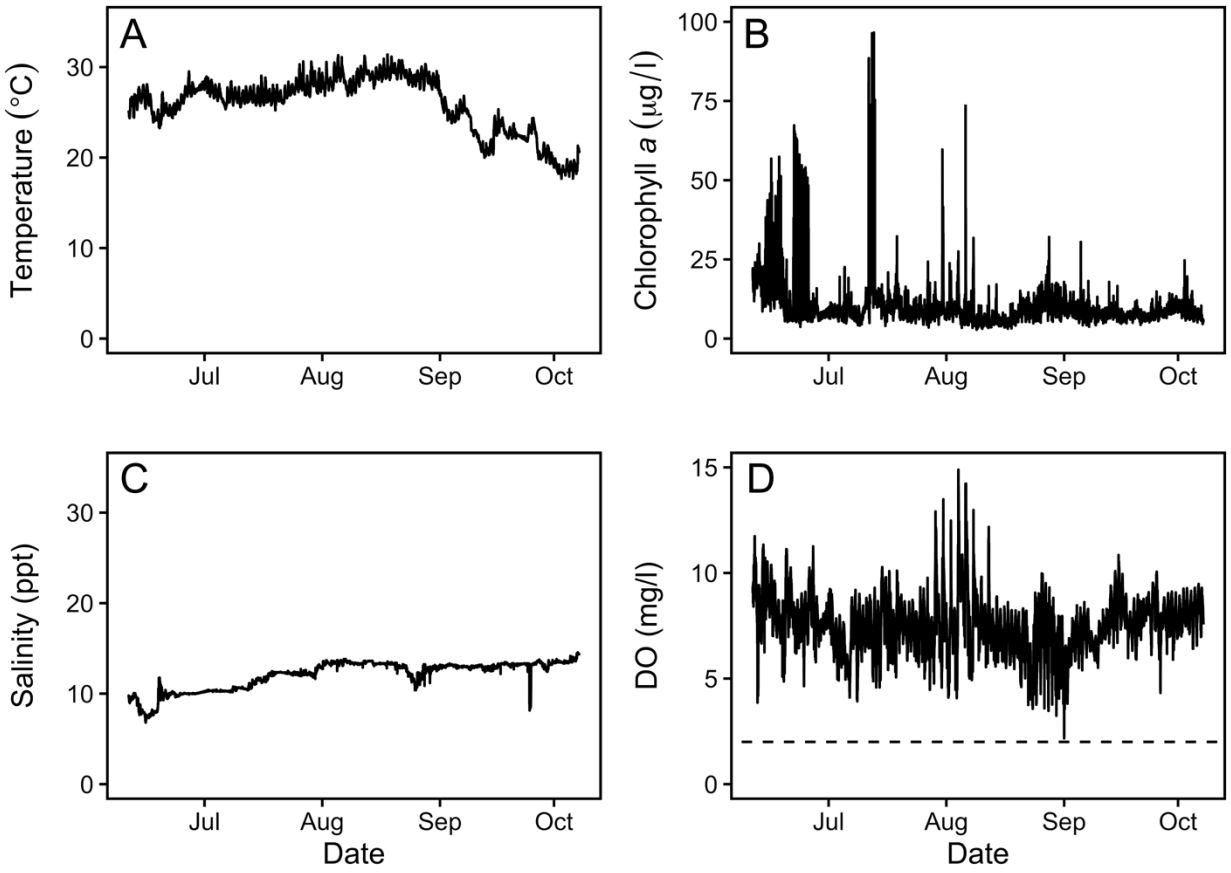

Supplementary Figure 5: Environmental data for the validation oyster growth dataset at Yeocomico River (YEO). A) Temperature (°C), B) Chlorophyll *a* (μg/l), C) Salinity (ppt) and D) Dissolved oxygen (mg/l). The dashed line on the dissolved oxygen panel correspond to 2.0 mg/l or hypoxic conditions.

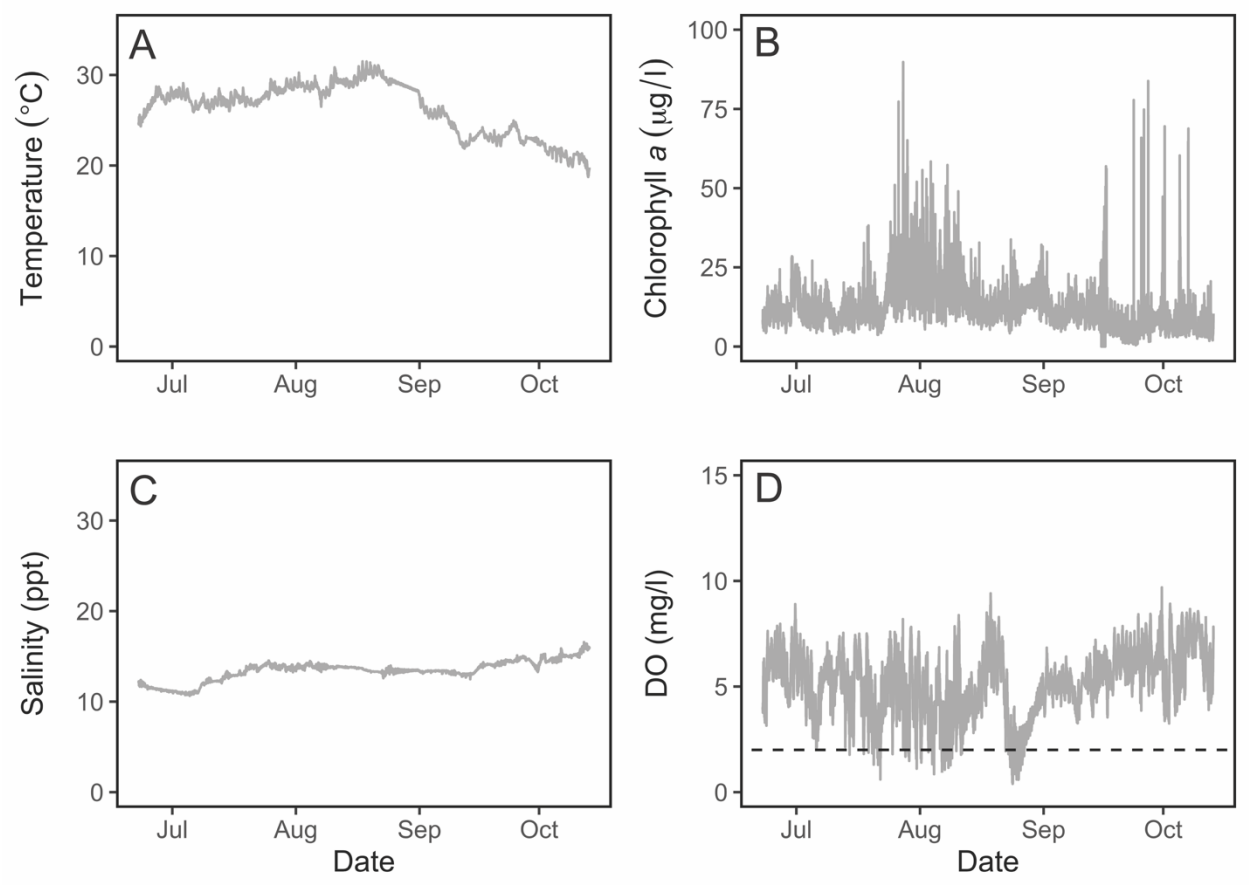

Supplementary Figure 6: Environmental data for the validation oyster growth dataset at Cole's Creek (CCR). A) Temperature (°C), B) Chlorophyll *a* (μg/l), C) Salinity (ppt) and D) Dissolved oxygen (mg/l). The dashed line on the dissolved oxygen panel correspond to 2.0 mg/l or hypoxic conditions.

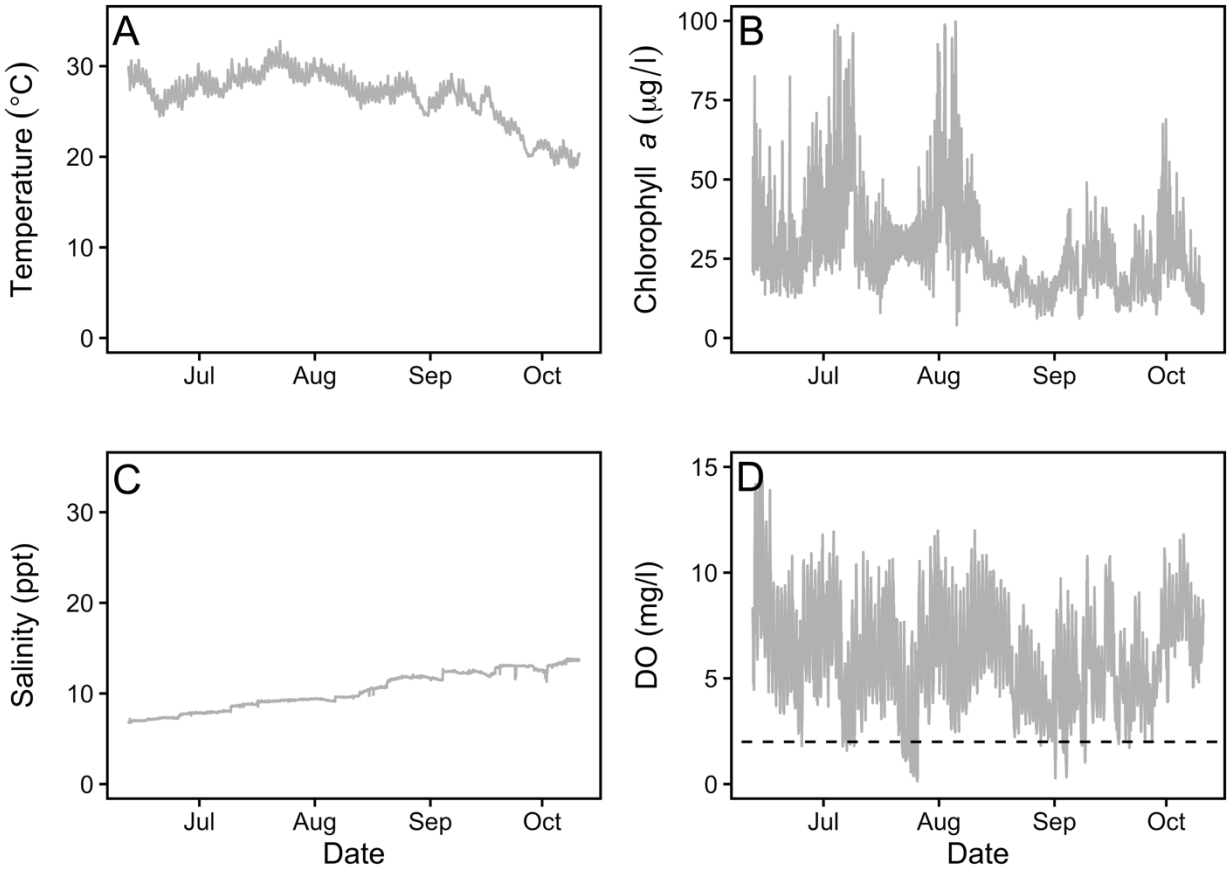

Supplementary Figure 7: Environmental data for the validation oyster growth dataset at Harness Creek (HCR). A) Temperature (°C), B) Chlorophyll *a* (μg/l), C) Salinity (ppt) and D) Dissolved oxygen (mg/l). The dashed line on the dissolved oxygen panel correspond to 2.0 mg/l or hypoxic conditions.

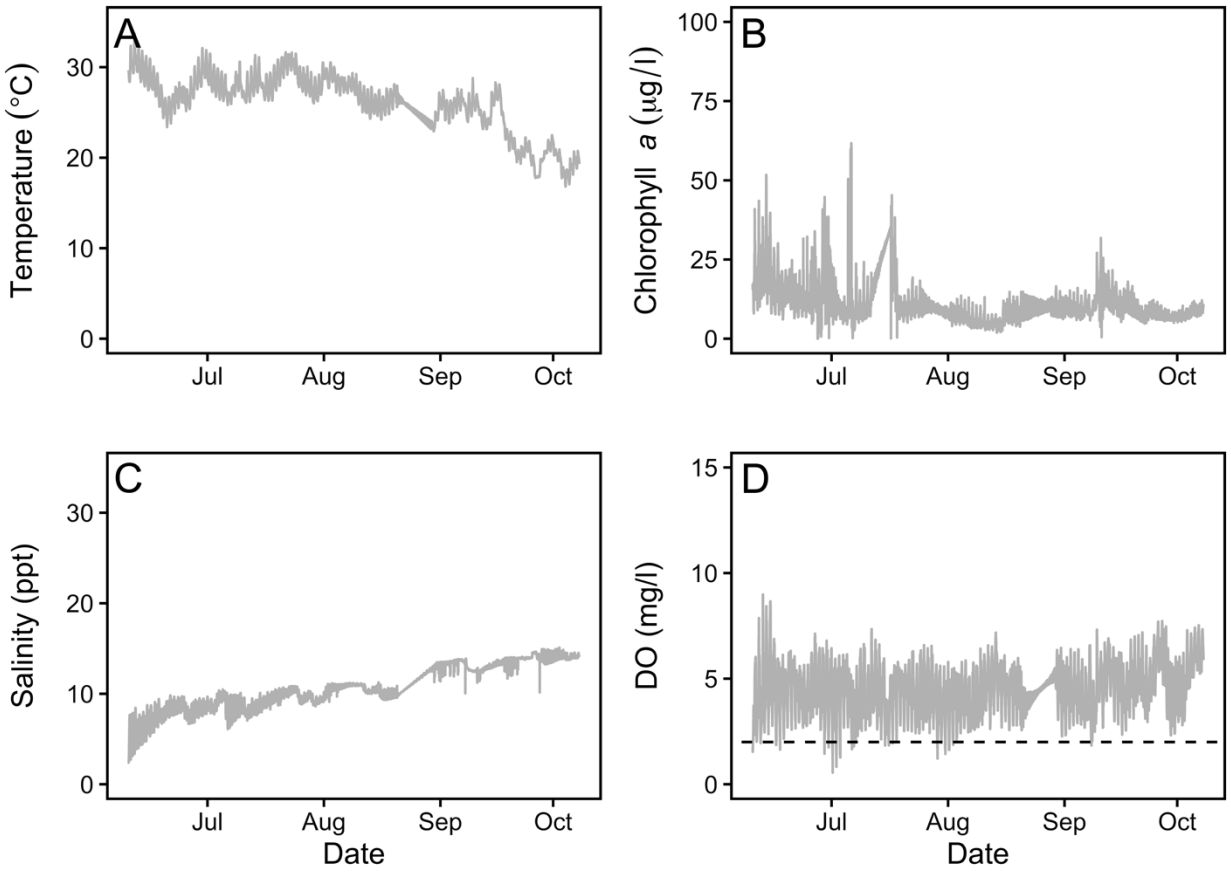

Supplementary Figure 8: Environmental data for the validation oyster growth dataset at Little Monie Creek (LMN). A) Temperature (°C), B) Chlorophyll *a* (μg/l), C) Salinity (ppt) and D) Dissolved oxygen (mg/l). The dashed line on the dissolved oxygen panel correspond to 2.0 mg/l or hypoxic conditions.

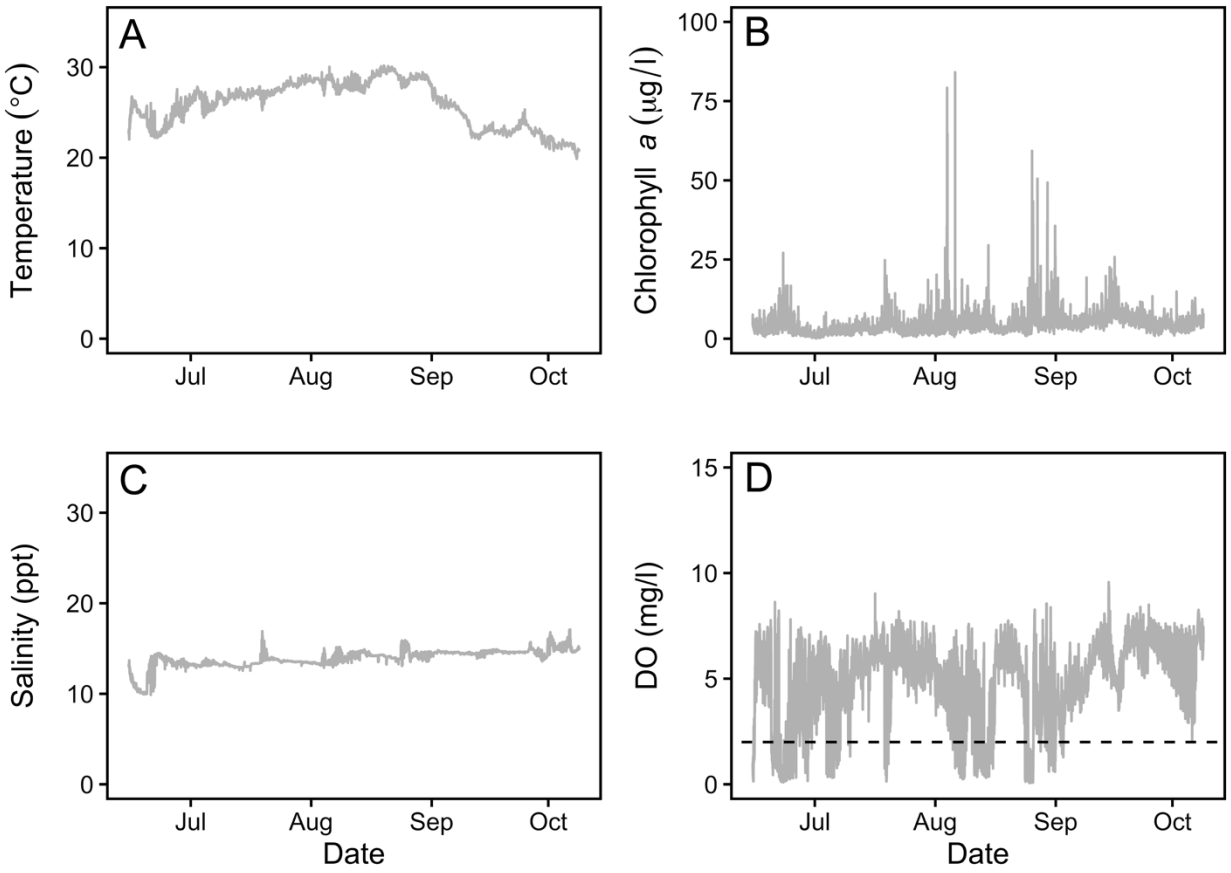

Supplementary Figure 9: Environmental data for the validation oyster growth dataset at St. Mary's College (SMC). A) Temperature (°C), B) Chlorophyll *a* (μg/l), C) Salinity (ppt) and D) Dissolved oxygen (mg/l). The dashed line on the dissolved oxygen panel correspond to 2.0 mg/l or hypoxic conditions.

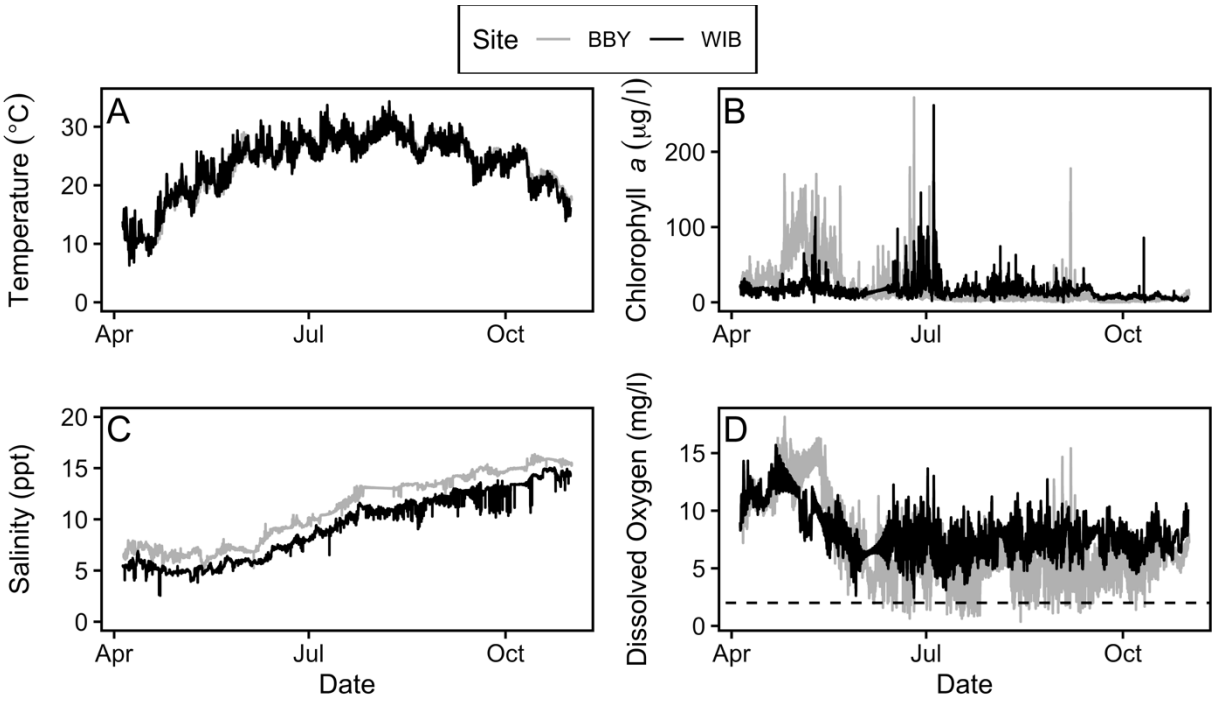

Supplementary Figure 10: Environmental data for predicted oyster growth at Wicomico Beach (WIB; black) and Breton Bay (BBY; grey). A) Temperature (°C), B) Chlorophyll *a* (μg/l), C) Salinity (ppt) and D) Dissolved oxygen (mg/l). The dashed line on the dissolved oxygen panel correspond to 2.0 mg/l or hypoxic conditions.